

## Electronic Supplementary Information for

### **Rational Design of Three-Dimensional Nitrogen-Doped Carbon Nanoleaf Networks for High-Performance Oxygen Reduction**

**Liang Chen<sup>§</sup>, Chenyu Xu<sup>§</sup>, Ran Du<sup>#</sup>, Yueyuan Mao<sup>§</sup>, Cheng Xue<sup>§</sup>, Liming Chen<sup>§</sup>,  
Liangti Qu<sup>§</sup>, Jin Zhang<sup>#</sup> and Tao Yi<sup>\*§</sup>**

[§] Department of Chemistry and Concerted Innovation Center of Chemistry for Energy Materials, Fudan University, 220 Handan Road, Shanghai 200433 (China).

E-mail: [yitao@fudan.edu.cn](mailto:yitao@fudan.edu.cn)

[§] Key Laboratory of Cluster Science, Ministry of Education of China, Beijing Key Laboratory of Photoelectronic/Electrophotonic Conversion Materials, Department of Chemistry, School of Science, Beijing Institute of Technology, Beijing 100081, P. R. China.

[#] Center for Nanochemistry, Beijing National Laboratory for Molecular Sciences, Key Laboratory for the Physics and Chemistry of Nanodevices, State Key Laboratory for Structural, Chemistry of Unstable and Stable Species, College of Chemistry and Molecular Engineering, Peking University, Beijing, 100871, P.R. China.

## Experimental Section

**Synthesis of CNT@GONRs.** CNT@GONRs was synthesized by longitudinally unzipping the multi-walled CNTs. Generally, pristine MWCNTs (1 g) (purified by calcination at 500 °C for 1 h and then washed repeatedly with HCl/HNO<sub>3</sub> to eliminate metal impurities before use) were mixed with concentrated sulphuric acid (250 mL) in a flask and stirred for 2 hours at room temperature. Then phosphoric acid (28 mL) was slowly added into the mixture and stirred for another 30 min. After that, different reaction solutions were then produced by the addition of 3 g and 4 g of powdered potassium permanganate at a rate of 1.5 g per hour until it was used out completely. After stirring for 1 h at room temperature, the reaction mixture was then heated at 70 °C for 2 h and then cooled to room temperature. Thereafter the mixture was poured into 400 mL of ice containing H<sub>2</sub>O<sub>2</sub> (30 %, 10 mL). The product was allowed to coagulate for one night and then washed with 5 wt% HCl solution, followed by centrifugation and dialysis process to remove the inorganic acid and all impurities. The final solution was concentrated to 10 mg mL<sup>-1</sup> and ultrasound for 30 minutes.

**Preparation of carbon nanoleaf frameworks.** Typically, 15 mL homogeneous CNT@GONRs<sub>25</sub> or CNT@GONRs<sub>85</sub> with a concentration of 10 mg mL<sup>-1</sup> and 5 vol% pyrrole (Py) aqueous dispersion (distilled before use) were mixed together by sonication for several minutes to form a uniform suspension, and sealed in a 20 mL Teflon-lined autoclave and maintained at 180 °C for 12 h. Then the autoclave was naturally cooled to room temperature to give the corresponding hydrogels. After solvent-exchanged with water and tert-butanol for a week to remove all impurities, freeze drying was used to remove the embedded solvents within the hydrogel to obtain the aerogels. Finally, the N-doped samples were prepared by heating these freeze-dried aerogels at 1030 °C for 2 h under Ar atmosphere. At this temperature, the Py or polypyrrole (PPy), if any, could form clean graphitic layer on GNRs/CNTs except those burned out and in situ doped into the GNRs layers.

**Synthesis of other analogue 3D N-doped catalysts (N-GNs/CNT-A and N-GNRs/CNT-A).** Graphene oxide (GO) and oxidized MWCNTs (ox-MWCNTs) were prepared according to methods reported elsewhere.<sup>s1, s2</sup> Typically, 8.5 mL 10 mg mL<sup>-1</sup> GNs or GONRs were mixed with 1.5 mL 10 mg mL<sup>-1</sup> ox-MWCNTs by sonication for several minutes to form a uniform suspension. After that, 5 vol% Py was added into the mixture and then sealed in a 20 mL Teflon-lined autoclave and maintained at 180 °C for 12 h. The following drying and pyrolysis procedures were similar with that of preparation of carbon nanoleaf frameworks described above.

**Characterization.** The structure of the obtained samples were characterized by XRD test by using monochromatic Cu K $\alpha$ 1 radiation ( $\lambda = 1.5406 \text{ \AA}$ ). The relative content of CNT and GNRs was

calculated from XRD patterns (Figure S2) by using the peak processing function of *OriginPro 8.0*. The peaks are selected from the position of the peak rising to the position of the peak completely dropping down. The BET specific area, pore size distribution and total pore volume data were obtained using ASAP 2010 (Micromeritics, USA) measurements at 77 K. Before measurement, all samples were degassed under vacuum at 200 °C for 10 h. XPS analysis was conducted using an AXIS Ultra spectrometer with a high-performance Al monochromatic source operated at 15 kV, and the peak processing of XPS was conducted using a *XPSPEAK41* software. Raman spectroscopy measurements were carried out on an XploRA Raman imaging microscope system with an excitation wavelength of 532 nm. TGA was carried out using a Pyris 1 TGA thermal analyzer from room temperature to 800 °C with 10 °C min<sup>-1</sup> heating rate in air or N<sub>2</sub> atmosphere. FESEM and TEM were recorded on an Ultra 55 and FEI Tecnai 20 at 200 KV. The test samples for TEM test was prepared by dissolving the aerogel samples in ethanol and then ultrasound for 30 minutes. After that, 20 μL suspensions was taken out using microsyringe and then dropped in a copper online. A Keithley 4200 Semiconductor Characterization System was used to measure the electrical conductivity (two-probe method) of the samples taken from the original as-prepared 3D-aerogel (cylinder shape). The calculation formulas are described below:

$$R = (\rho l)/S; \quad \kappa = 1/\rho; \quad S = \pi \cdot (d/2)^2$$

$R$  is the resistance of the samples;  $\rho$  is the resistivity of the samples;  $l$  is the length of the samples;  $d$  is the diameter of the samples;  $S$  is the surface area of the samples;  $\kappa$  is the electric conductivity of the samples.

Oxygen reduction reaction (ORR) measurements were carried out on an electrochemical workstation (CHI 760D) with a three-electrode system. The glassy-carbon (GC) rotating disk electrode (RDE) (diameter 5 mm) was used as working electrode with a Pt foil electrode and an Ag/AgCl with saturated KCl solution electrode as counter and reference electrode (calibrated and converted to RHE), respectively. Before the preparation of electrodes, a sample of 2 mg was first ultrasonically dispersed in 0.5 mL ethanol with 50 μL of Nafion solution (5%), then the mixed suspensions (~5 μL) were attached onto a glass carbon (GC) electrode (ca. ~0.25 cm<sup>2</sup>) as working electrode with the mass loading of 0.08 mg cm<sup>-2</sup>. Commercial Pt/C (20 wt% Pt on Vulcan XC-72) electrode with the similar amount (~20 μg) was prepared by the same procedure. Catalyst loadings for all samples, including Pt/C were 80 μg cm<sup>-2</sup>. 0.1 M KOH was saturated with O<sub>2</sub> by bubbling oxygen for 30 min before testing. For cyclic voltammetry test, the working electrode was cycled between -1.2 V and 0.2 V at a scan rate of 10 mV s<sup>-1</sup>. For control experiments in N<sub>2</sub> saturated KOH, using N<sub>2</sub> instead of O<sub>2</sub> while

other conditions remain unchanged. Measurements on a rotating ring-disk electrode (RRDE) and/or rotating disk electrode (RDE) were carried out on a MSR-X electrode rotator (Pine Instrument) and the CHI 760D potentiostat at 0.1 M KOH was used as the electrolyte. Rotating ring-disk electrode (RRDE) measurements were conducted at different rotating speed from 400 to 1600 rpm at a scan rate of 10 mV s<sup>-1</sup>. The transferred electron number ( $n$ ) was determined based on the Koutechy-Levich ( $K-L$ ) equation:

$$\frac{1}{J} = \frac{1}{J_L} + \frac{1}{J_K} = \frac{1}{B\omega^{1/2}} + \frac{1}{J_K} \quad (1)$$

$$B = 0.62nFC_o(D_o)^{2/3}\nu^{-1/6} \quad J_K = nFkC_o \quad (2)$$

Here  $J$  represents the measured current density,  $J_K$  and  $J_L$  are the kinetic and diffusion-limiting current density,  $\omega$  is the electrode rotating rate,  $n$  is the electron transfer number,  $F$  is the Faraday constant ( $F = 96485 \text{ C mol}^{-1}$ ),

$D_o$  is the diffusion coefficient of O<sub>2</sub> in 0.1 M KOH ( $D_o = 1.9 \times 10^{-5} \text{ cm}^2 \text{ s}^{-1}$ ),  $C_o$  is the bulk concentration of O<sub>2</sub> ( $C_o = 1.2 \times 10^{-6} \text{ mol cm}^{-3}$ ) and  $\nu$  is the kinetic viscosity ( $\nu = 0.01 \text{ cm}^2 \text{ s}^{-1}$ ). The constant 0.2 is adopted when the rotation rate is expressed in rpm. For the Tafel plot, the kinetic current was calculated from the mass-transport correction of RDE by:

$$J_K = J \times J_L / (J_L - J)$$

The  $n$  was also determined from the RRDE measurement:

$$n = 4I_d / (I_d + I_r / N) \quad (3)$$

The peroxide percentage (% HO<sub>2</sub><sup>-</sup>) was calculated based on the equation:

$$\% \text{HO}_2^- = 200 \times I_r / N / (I_d + I_r / N) \quad (4)$$

Here  $I_d$  and  $I_r$  is the disk current and ring current, respectively, and  $N$  is the current collection efficiency of Pt ring and determined to be 0.37.

To remove the capacitive current of the working electrode, the background current was measured by running the rotating-disk electrode in N<sub>2</sub>-saturated 0.1 M KOH electrolyte after ORR measurements and was subtracted from the ORR polarization curve. Therefore, we use the net Faradic current of ORR to evaluate the ORR activity of our materials.

**Table S1. Representative heteroatom-doped porous carbon-based electrocatalysts for the ORR in alkaline medium.**

Electrocatalysts	Loadings ( $\mu\text{g cm}^{-2}$ )	Heteroatom content (atom %)	Onset potential (vs Ag/AgCl)	Electron transfer number ( <i>n</i> )	Maximum HO <sub>2</sub> <sup>-</sup> %	Ref.
<b>N-CNT@GNRs85-A</b>	<b>80</b>	<b>N: 2.79 %</b>	<b>0.04 V</b>	<b>3.89-3.96</b>	<b>5.5 %</b>	<b>Present work</b>
<b>N-CNT@GNRs25-A</b>	<b>80</b>	<b>N: 2.17 %</b>	<b>0.03 V</b>	<b>3.87-3.94</b>	<b>6.45 %</b>	<b>Present work</b>
NGNRs-A	80	N: 2.81 %	-0.05 V	3.71-3.96	14.7 %	[s3]
N-doped graphene <b>1</b>	50.91	N: 5.0 %	-0.03 V	3.70 at -0.4 V	Unknown	[s4]
N-doped graphene <b>2</b>	40	N: 7.1 %	-0.10 V	3.4~3.6	≈29.6 %	[s5]
Amino-functionalize graphene	51	N: 10.6 %	-0.04V	3.1~3.4	≈44.5 %	[s6]
N-doped graphene <b>3</b>	Unknown	N: 6.65 %	-0.13 V	3.2~3.5	≈40 %	[s7]
N-doped graphene <b>4</b>	141	N: 8.05 %	-0.10 V	3.3~3.7	≈34.7 %	[s8]
N-GQDs	141	N: 4.28 %	-0.16 V	3.6~4.4	≈20 %	[s9]
N-doped graphene <b>5</b>	141	N: 7.86 %	-0.10 V	3.6~4.0	≈20 %	[s10]
3D GF	12	N: 4.9 %	-0.18 V	3.7	< 20 %	[s11]
N-doped graphene <b>6</b>	38	N: 4.6 %	-0.04 V	3.2 at -0.8 V	Unknown	[s12]
N-doped G/CNT	51	N: 7.76 %	-0.14 V	3.3~3.7	≈34.7 %	[s13]
N-graphene/CNT	Unknown	N: 6.6 %	-0.08 V	3.98 at -0.25 V	Unknown	[s14]
N, S-doped graphene	Unknown	N: 4.5 %; S:2.0 %	-0.06 V	3.3~3.6	≈34.7 %	[s15]
S-doped Nanoplatelets	76	S: 4.94 %	-0.22 V	3.3	Unknown	[s16]
N-doped GNRs	50	N: 8.3 %	-0.21 V	3.91	Unknown	[s17]
N-doped carbon nanocages	80	N: 4.5 %	-0.13 V	3.27	Unknown	[s18]
S, N-doped carbon	306	N: 4.7 %; S: 0.68 %	-0.05 V	4.0 at -0.3V	Unknown	[s19]
N,S-doped few layers graphene oxide	306	N: 8 %; S:3.2 %	-0.11 V	3.7	Unknown	[s20]
N-S-GMF	80	N: 5.1 %; S: 0.99 %	0.04 V	3.7	<15 %	[s21]
B,N-doped graphene	Unknown	B: 2.1 % N: 3.1 %	-0.16 V	3.4~3.8	≈29.6 %	[s22]
VA-BCN	Unknown	B: 4.2 % N: 10.3 %	Unknown	3.7-4.0	<15 %	[s23]
N-doped CNT arrays	Unknown	N: 6.1 %	-0.22 V	3.9 at -0.3 V	Unknown	[s24]
N-doped carbon nanosheets	600	N: 3.5 %	-0.01 V	3.67-3.94	≈16.5 %	[s25]
Porous carbon	110	N: 1.55 %	-0.02 V	3.49-3.67	≈25.5 %	[s26]
N-doped carbons	820	N: 12 %	0.035 V	3.2	Unknown	[s27]
N-doped Carbon Capsules	657	N: 15 %	-0.06 V	3.75-4.0	<16.0 %	[s28]
N-OMMC-G	417	Unknown	-0.05 V	Unknown	Unknown	[s29]

The maximum peroxide percentage (%) in the reference samples was calculated based on the equation (3) and (4) mentioned above.

## Additional figures

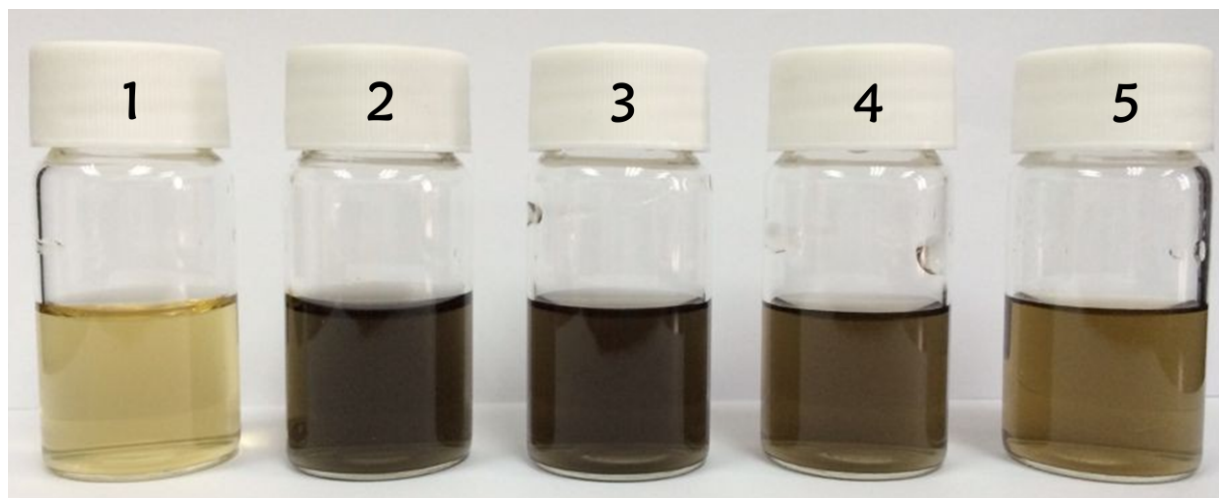


**Fig. S1** The digital photos of the carbon-based solutions used in this work. The concentration of these solutions is  $0.05 \text{ mg mL}^{-1}$ . **(1)** Graphene oxide prepared by modified Hummers methods [*J. Mater. Chem.*, **2012**, *22*, 22090-22096], **(2)** oxidized multi-walled carbon nanotubes (ox-MWCNTs), **(3)** CNT@GONRs25, **(4)** CNT@GONRs85, **(5)** Pure GONRs.

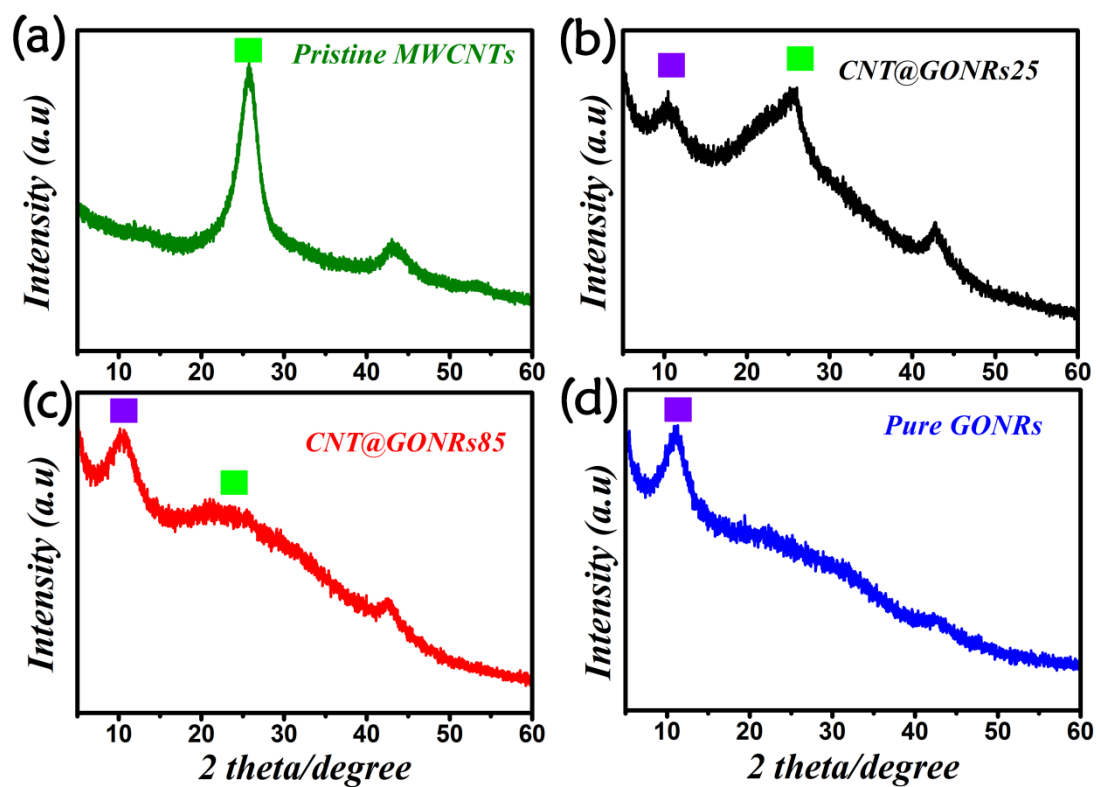


**Fig. S2** XRD patterns of (a) pristine MWCNTs, (b) CNT@GONRs25, (c) CNT@GONRs85 and (d) Pure GONRs. The purple rectangle appears in (a-d) represents the peak position of carbon nanotube, and the light green rectangle represents the peak position of graphene oxide nanoribbons.

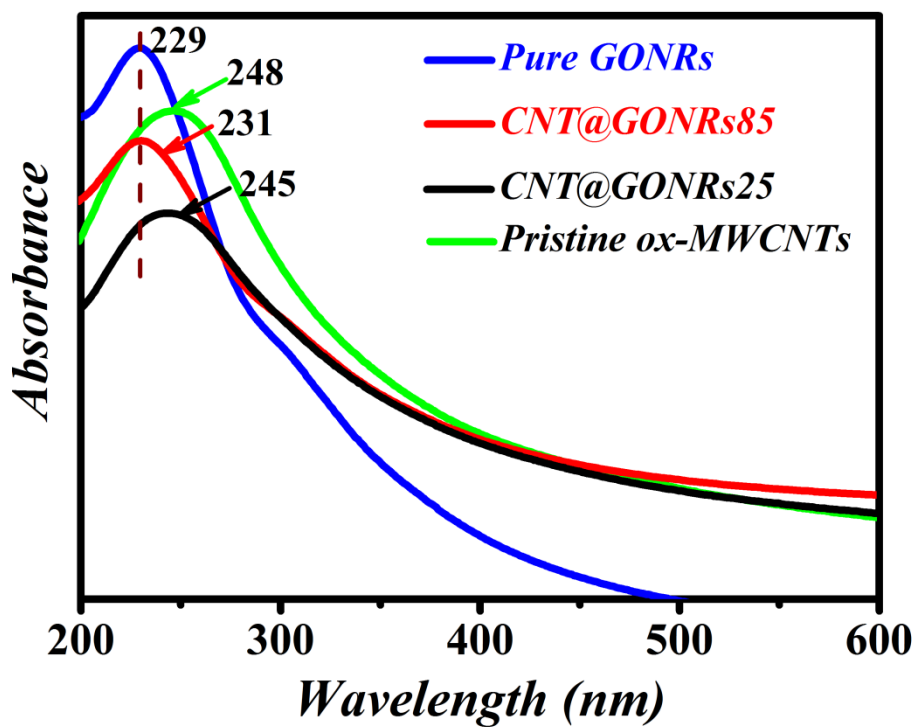


**Fig. S3** UV-Vis spectra of pristine ox-MWCNTs, CNT@GONRs 25, CNT@GONRs85 and Pure GONRs.

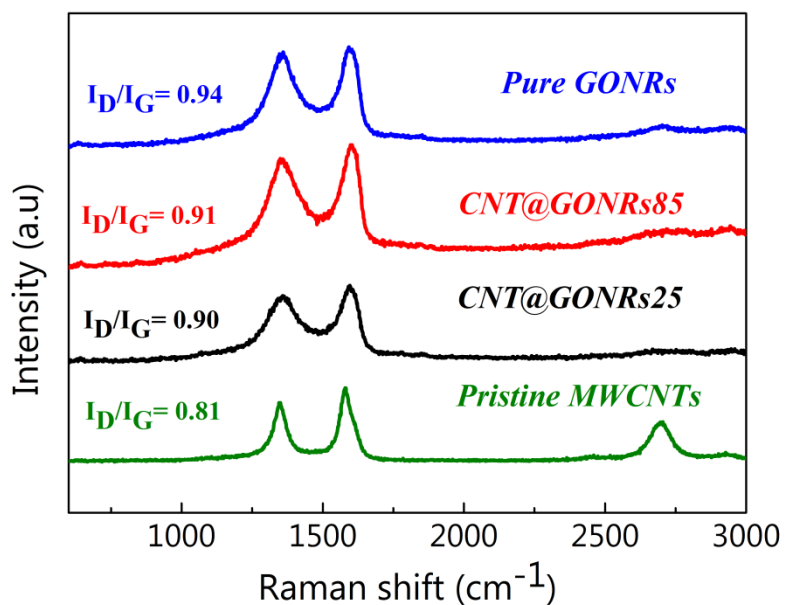


**Fig. S4** Raman spectra of pristine MWCNTs, CNT@GONRs25, CNT@GONRs85 and Pure GONRs.

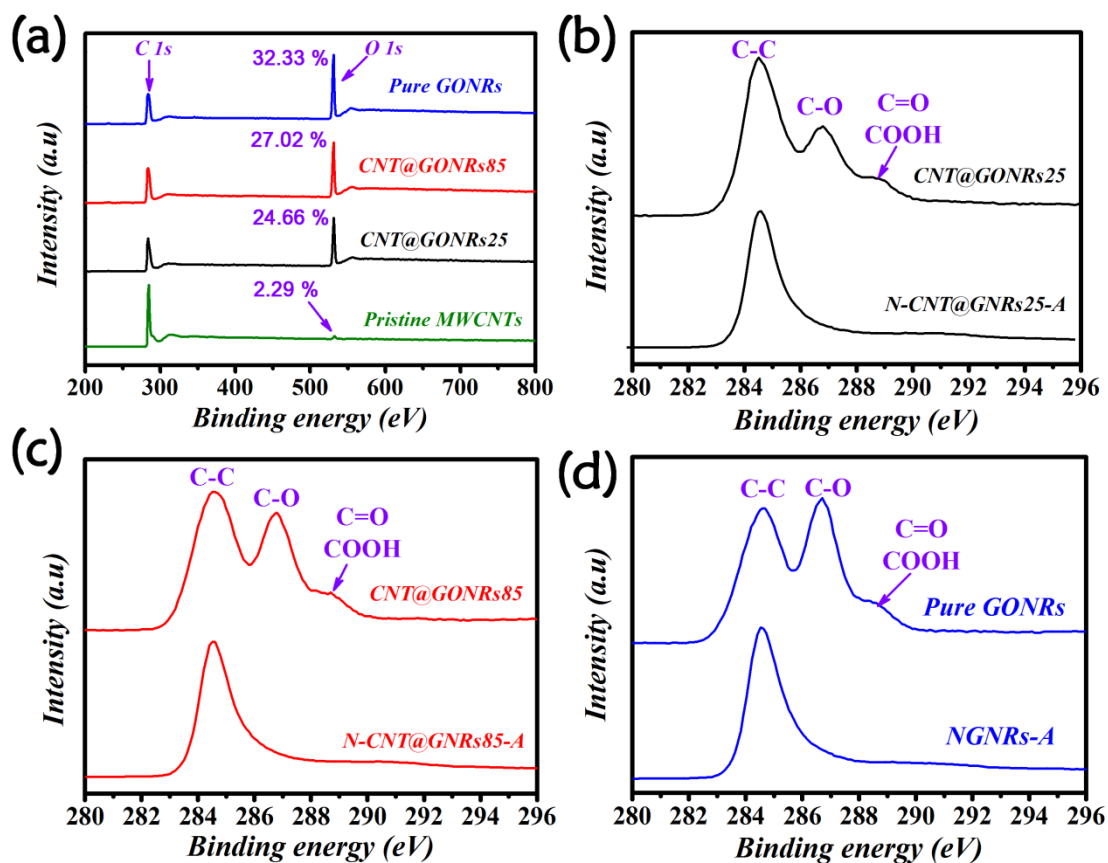


**Fig. S5** (a) XPS survey profiles of the pristine MWCNTs, CNT@GONRs 25, CNT@GONRs85 and Pure GONRs. High-resolution C 1s spectrum of (b) CNT@GONRs25 and corresponding N-CNT@GONRs25-A; (c) CNT@GONRs85 and corresponding N-CNT@GONRs85-A; (d) Pure GONRs and corresponding NGNRs-A.

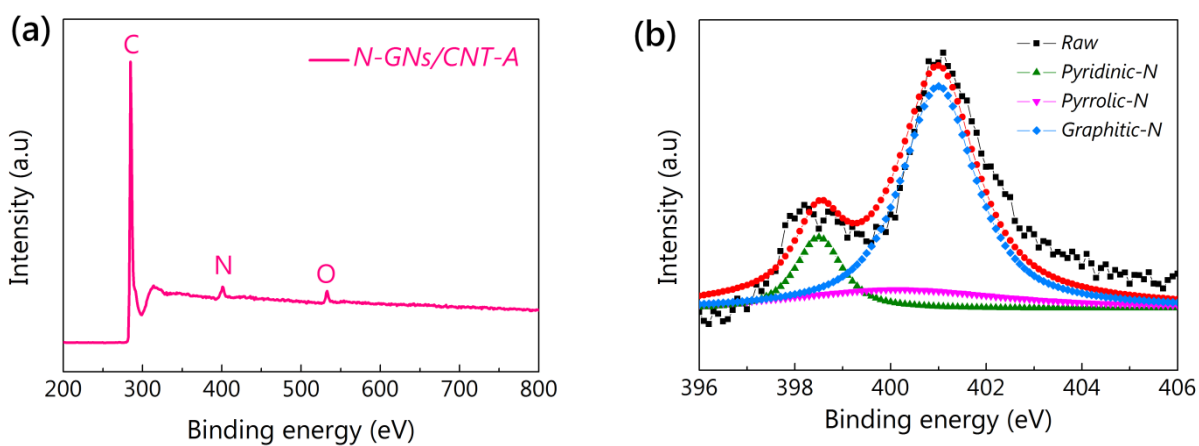


**Fig. S6 (a)** XPS spectrum of N-GNs/CNT-A and **(b)** the corresponding high-resolution N1s peak.

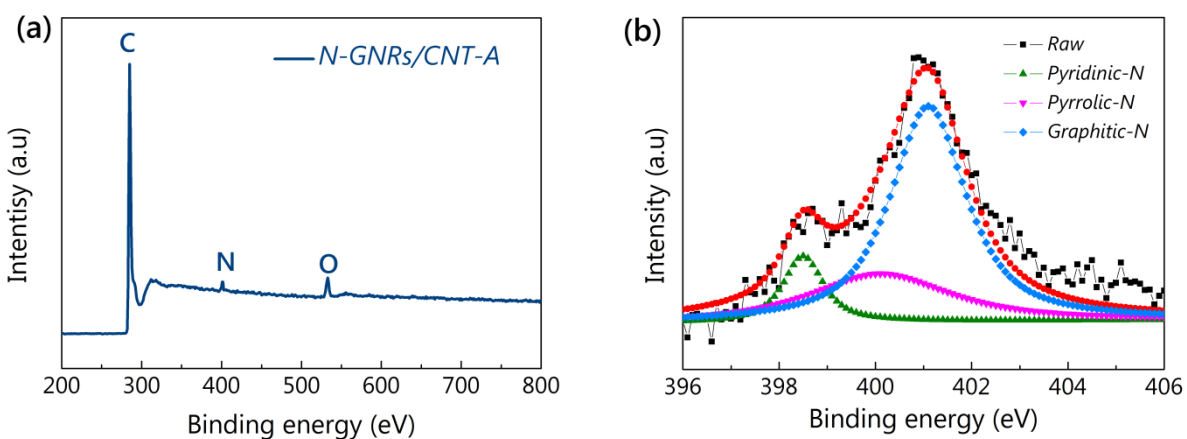


**Fig. S7 (a)** XPS spectrum of N-GNRs/CNT-A and **(b)** the corresponding high-resolution N1s peak.

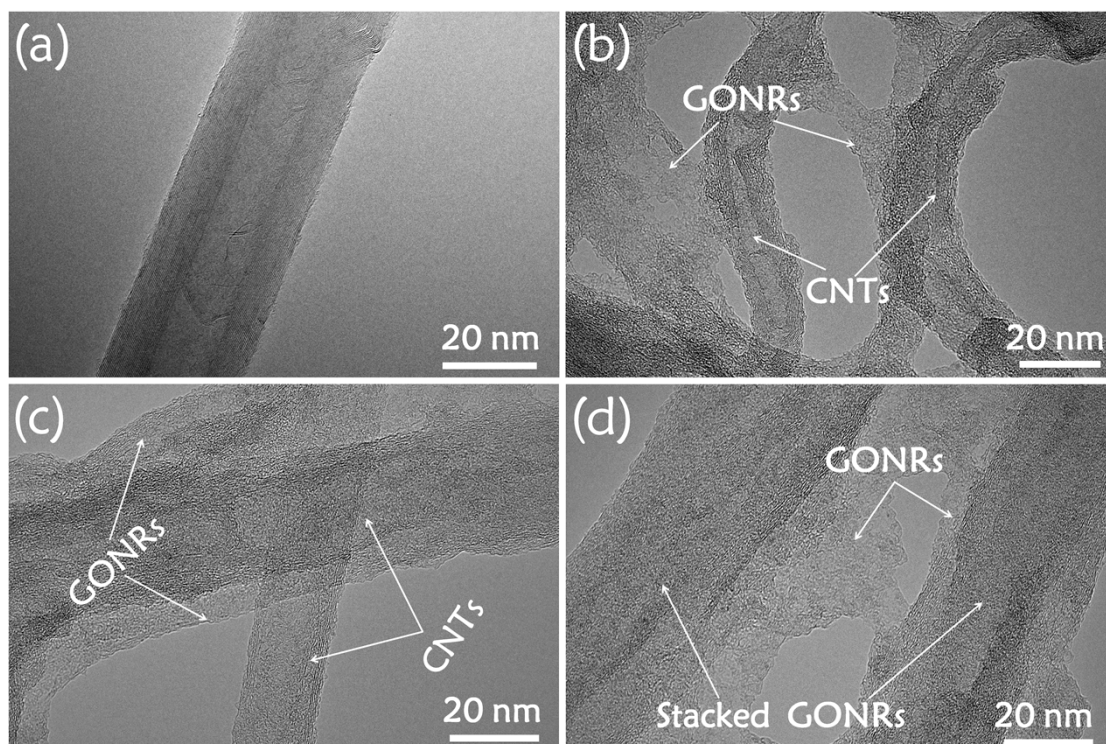


**Fig. S8** TEM images of (a) Pristine MWCNTs; (b) CNT@GONRs25; (c) CNT@GONRs85 and (d) pure GONRs.

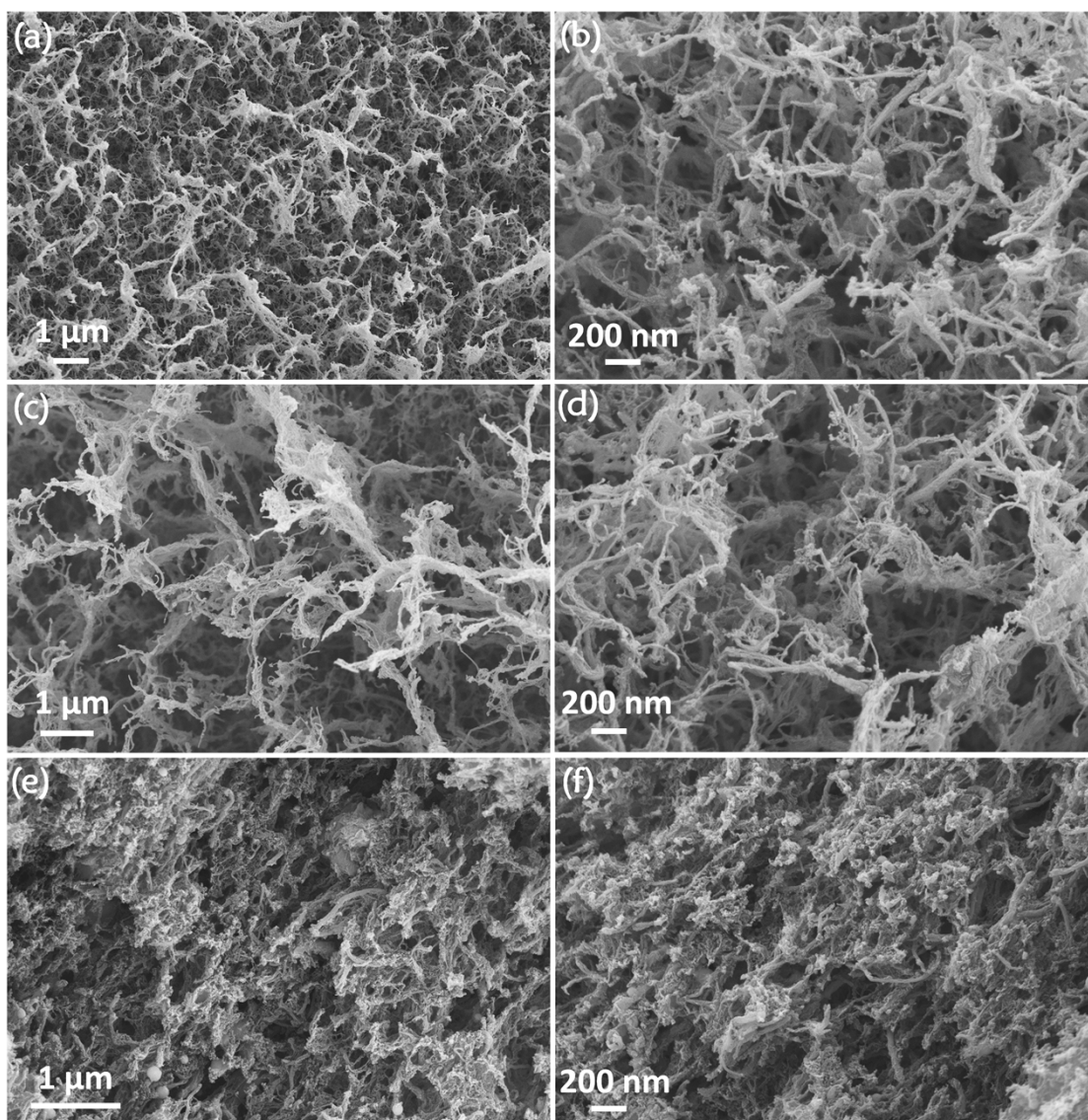


**Fig. S9** SEM images of the corresponding aerogels before pyrolysis process. **(a, b)** CNT@GNRs25-A; **(c, d)** CNT@GNRs85-A and **(e, f)** GNRs-A.

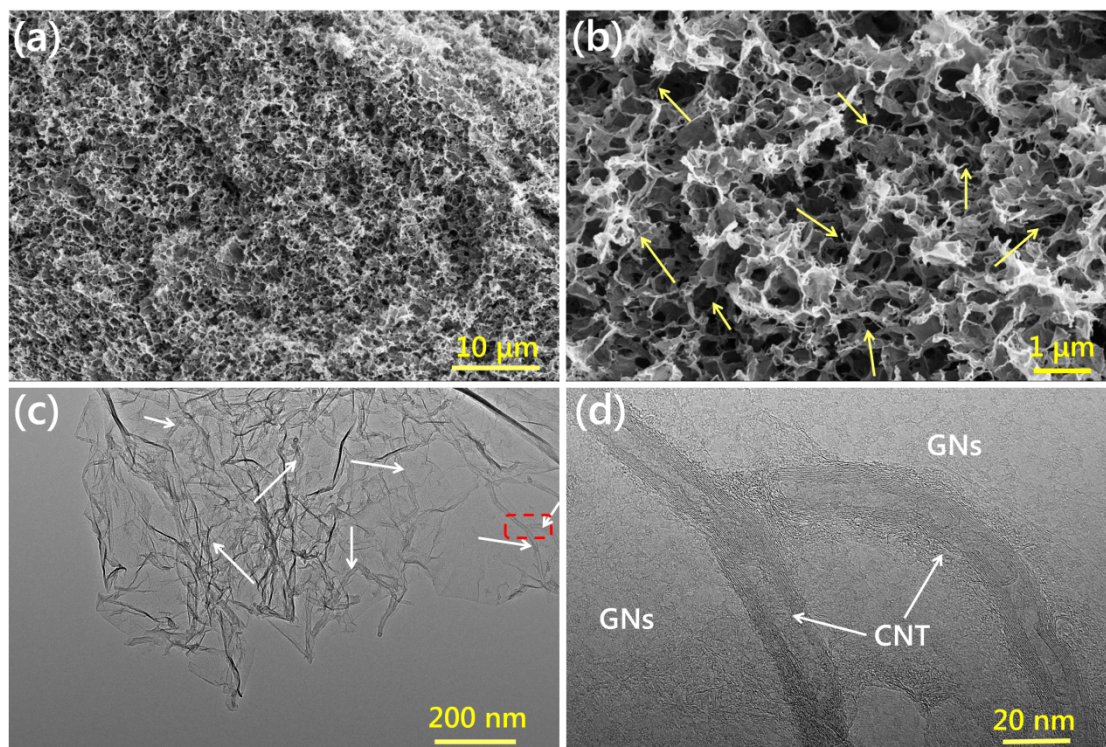


**Fig. S10 (a,b ) SEM and (c, d) TEM images of the analogy catalyst N-GNs/CNT-A.**

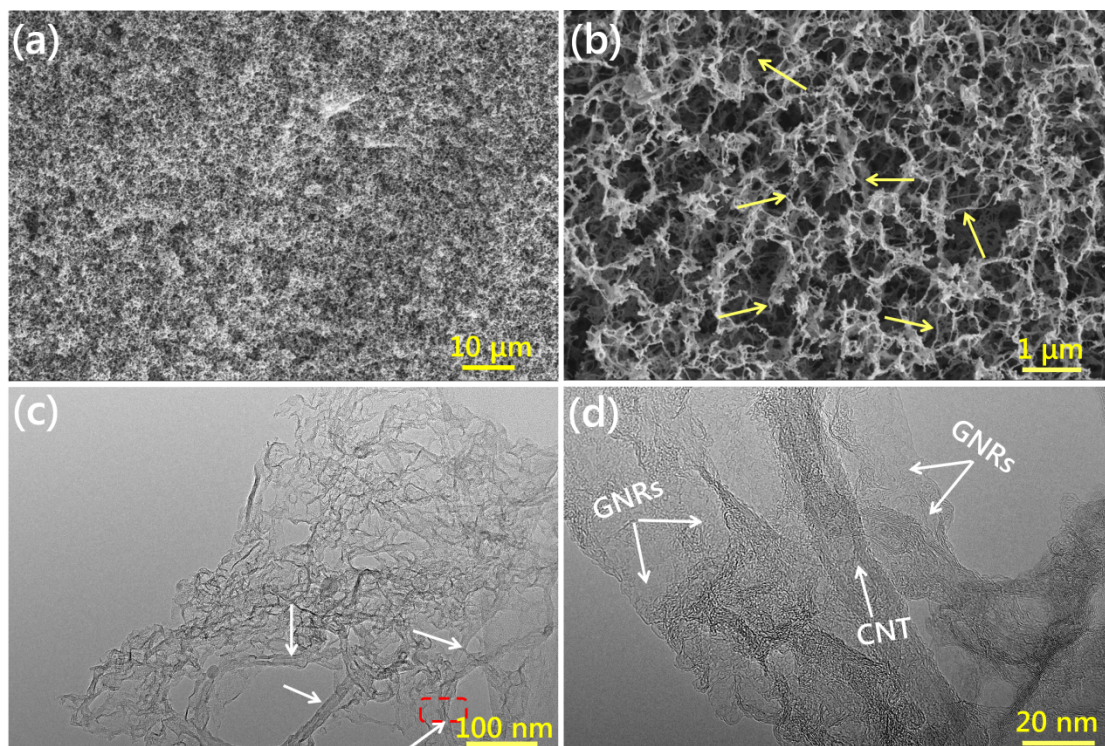


**Fig. S11 (a, b ) SEM and (c, d) TEM images of the analogy catalyst N-GNRs/CNT-A**

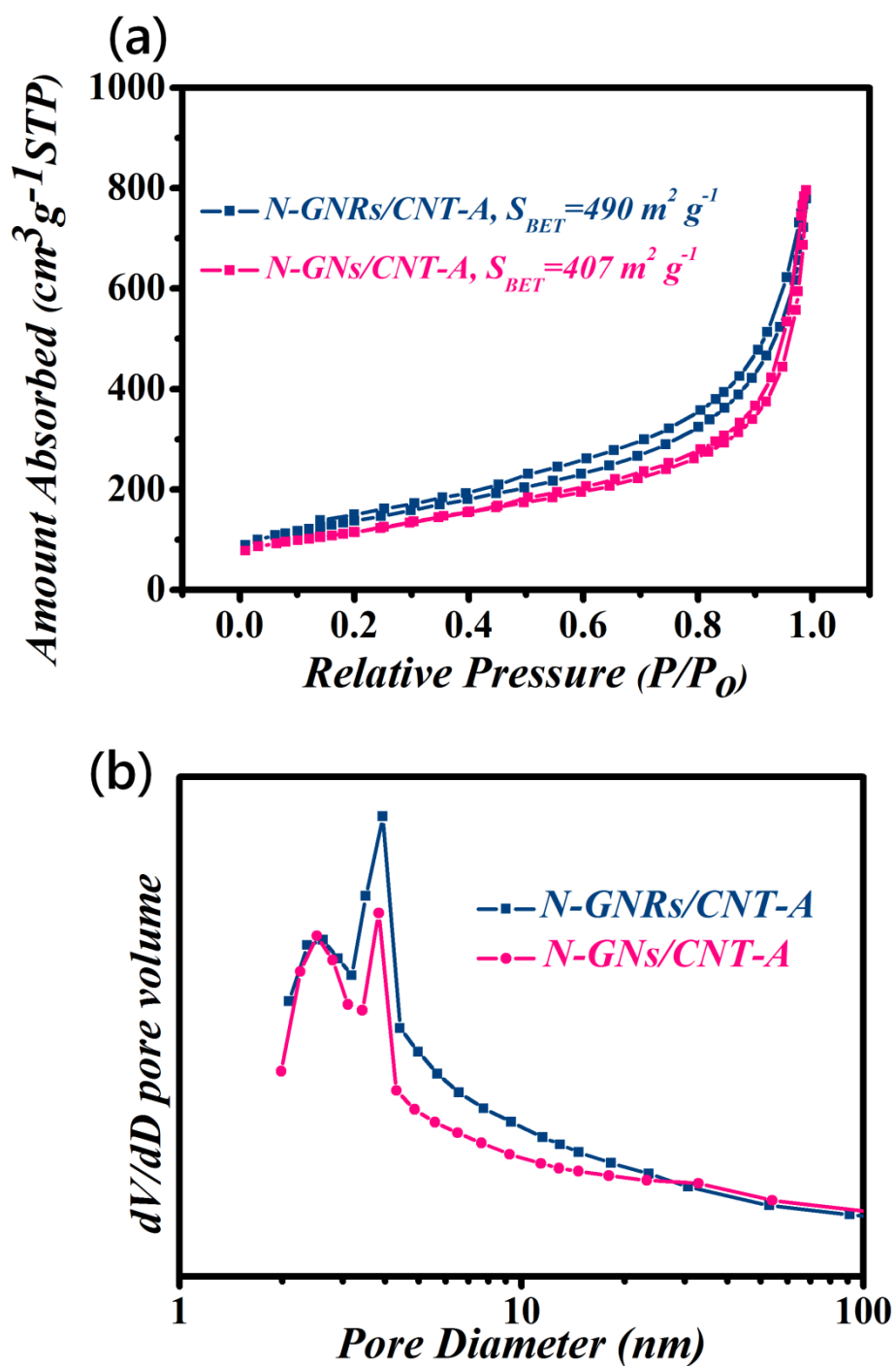


**Fig. S12** (a) Typical nitrogen adsorption-desorption isotherms and (b) BJH (Barret–Joyner–Halenda) pore size distribution curves of the resulting N-GNs/CNT-A and N-GNRs/CNT-A.

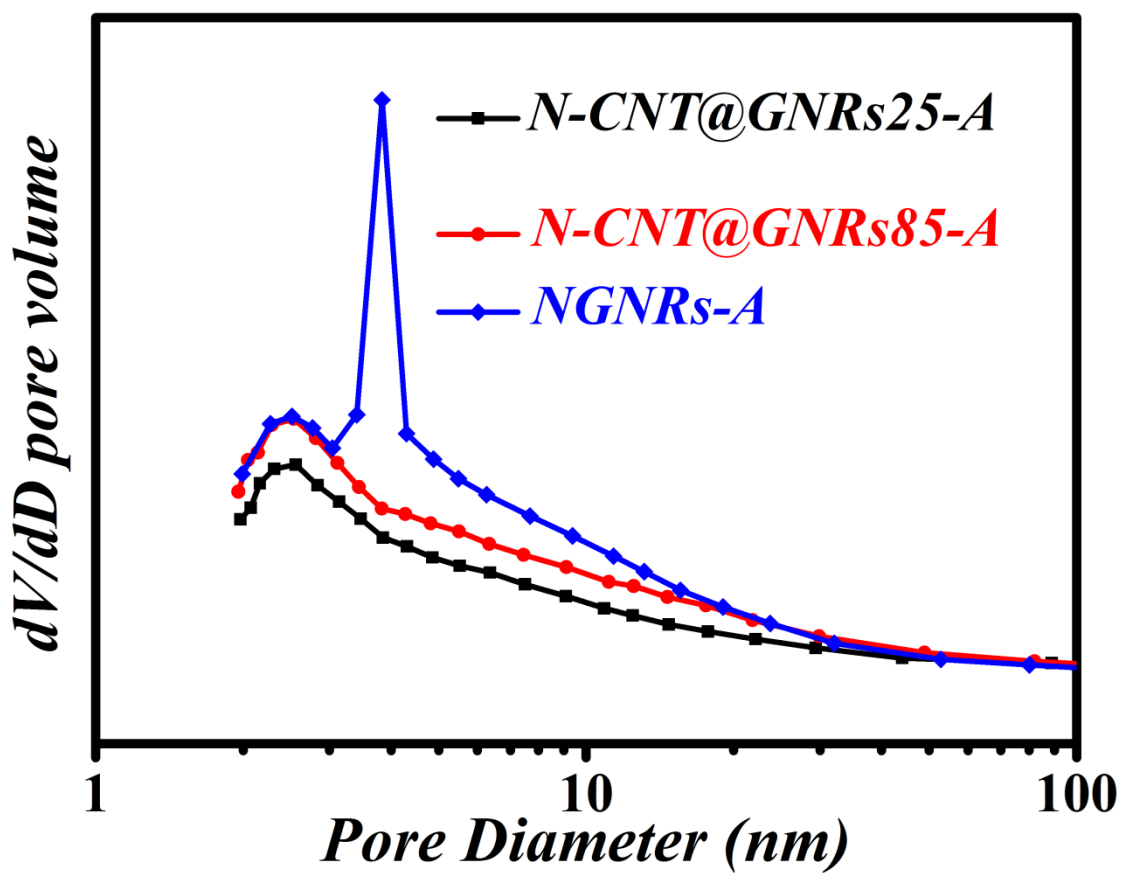


**Fig. S13** BJH (Barret–Joyner–Halenda) pore size distribution curves of the resulting N-CNT@GNRs25-A, N-CNT@GNRs85-A and NGNR-A.

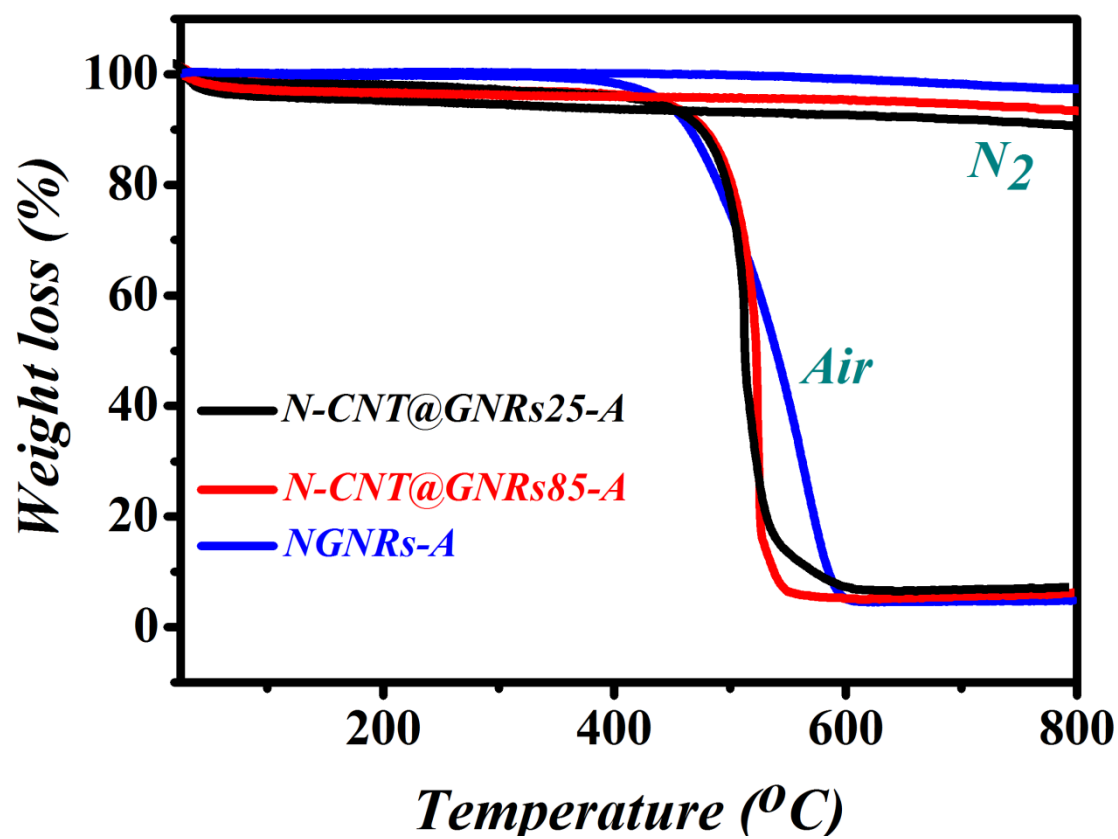


Fig. S14 TGA curves of the as-obtained N-CNT@GNRs25-A, N-CNT@GNRs85-A and NGNR-A.

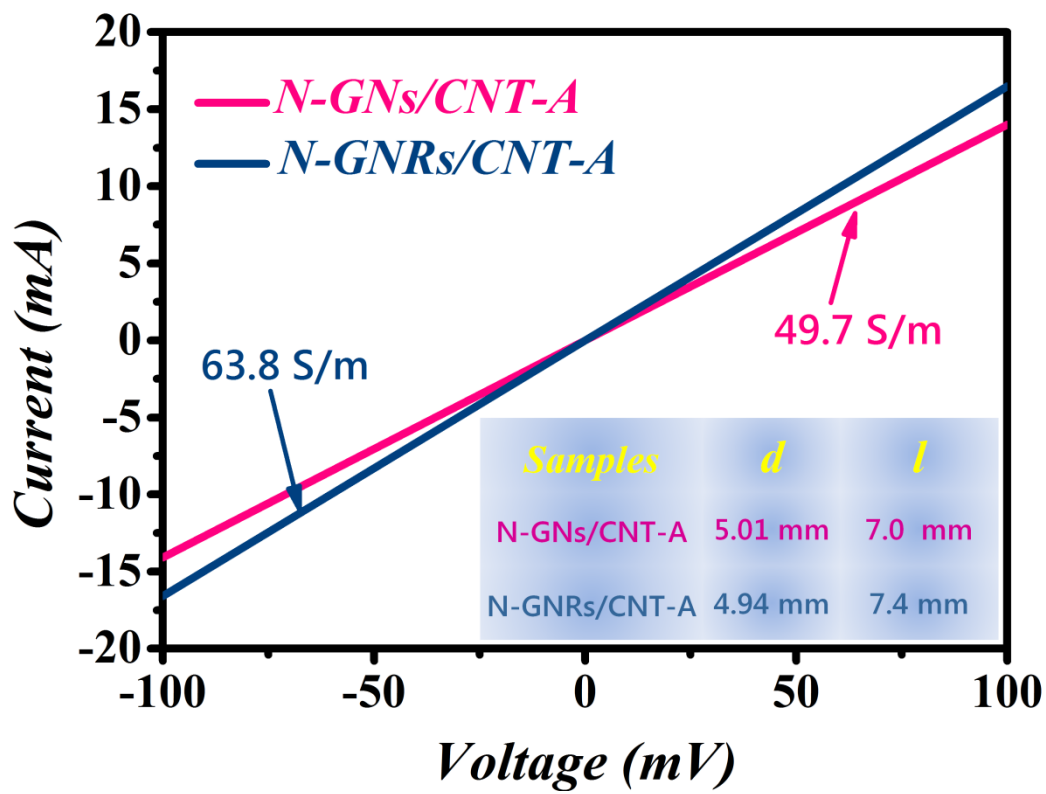
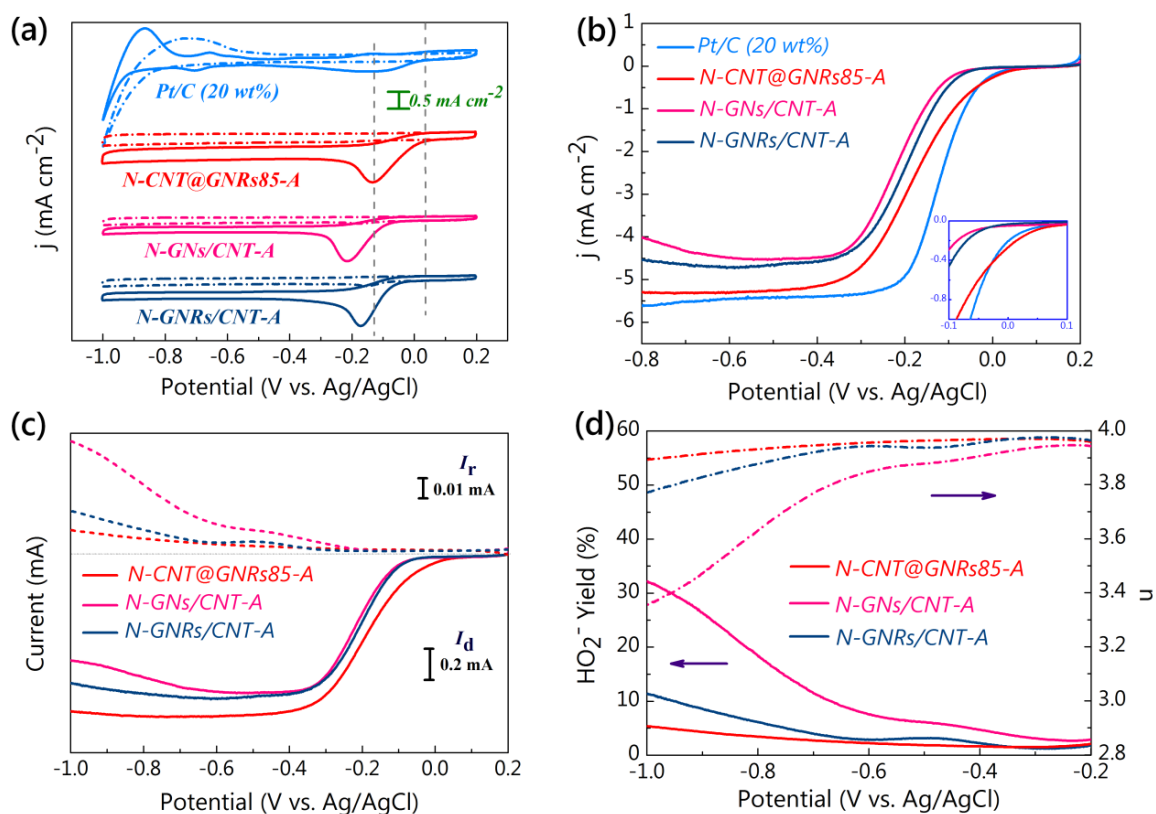
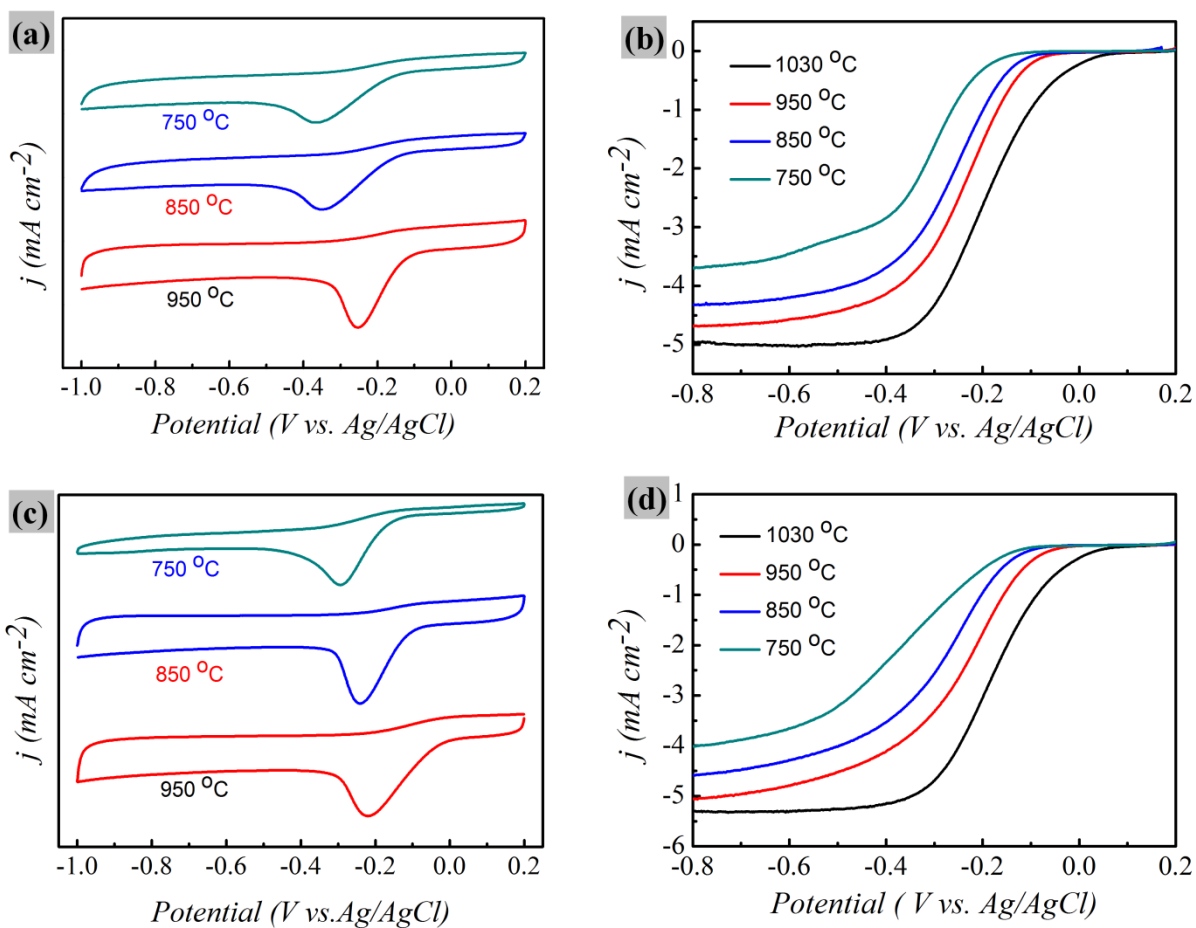


Fig. S15 Typical  $I$ - $V$  curves of N-GNs/CNT-A and N-GNRs/CNT-A.



**Fig. S16** (a) CV curves of as-prepared N-CNT@GNRs85-A, N-GNs/CNT-A, N-GNRs/CNT-A and Pt/C (20 wt%) in a  $N_2$ - and  $O_2$ -saturated 0.1 M KOH solution at a scanning rate of  $10\ mV\ s^{-1}$ . (b) LSV curves of the as-prepared N-CNT@GNRs85-A, N-GNs/CNT-A, N-GNRs/CNT-A and Pt/C in an  $O_2$ -saturated 0.1 M KOH solution at a scanning rate of  $10\ mV\ s^{-1}$  and a rotation speed of 1600 rpm. (c) Rotating ring-disk electrode curves of N-CNT@GNRs85-A, N-GNs/CNT-A, N-GNRs/CNT-A at 1600 rpm. (d) Peroxide percentage and electron transfer number ( $n$ ) of N-CNT@GNRs85-A, N-GNs/CNT-A, N-GNRs/CNT-A within the potential range of -1.0 V~-0.2 V.



**Fig. S17** CV and LSV curves of the N-CNT@GNRs25-A **(a-b)** and N-CNT@GNRs85-A **(c-d)** samples obtained by annealing at 950 °C, 850 °C and 750 °C for 3 hours.

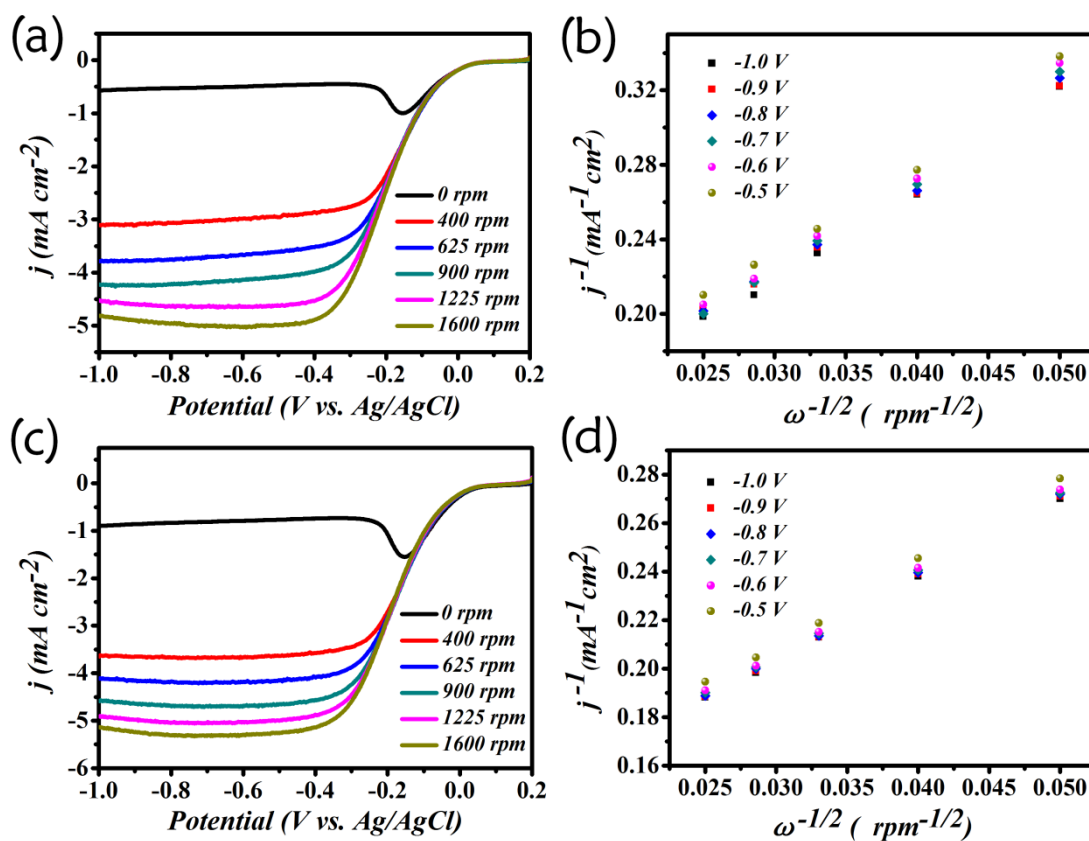


**Fig. S18** RDE curves of (a) N-CNT@GNRs25-A and (c) N-CNT@GNRs85-A in an O<sub>2</sub>-saturated 0.1 M KOH solution with various rotation speeds at a scanning rate of 10 mV s<sup>-1</sup>. K-L plots of  $J^{-1}$  vs.  $\omega^{-1/2}$  of (b) N-CNT@GNRs25-A and (d) N-CNT@GNRs85-A at different electrode potentials derived from RDE measurements (with mass loading of 0.08 mg cm<sup>-2</sup>).

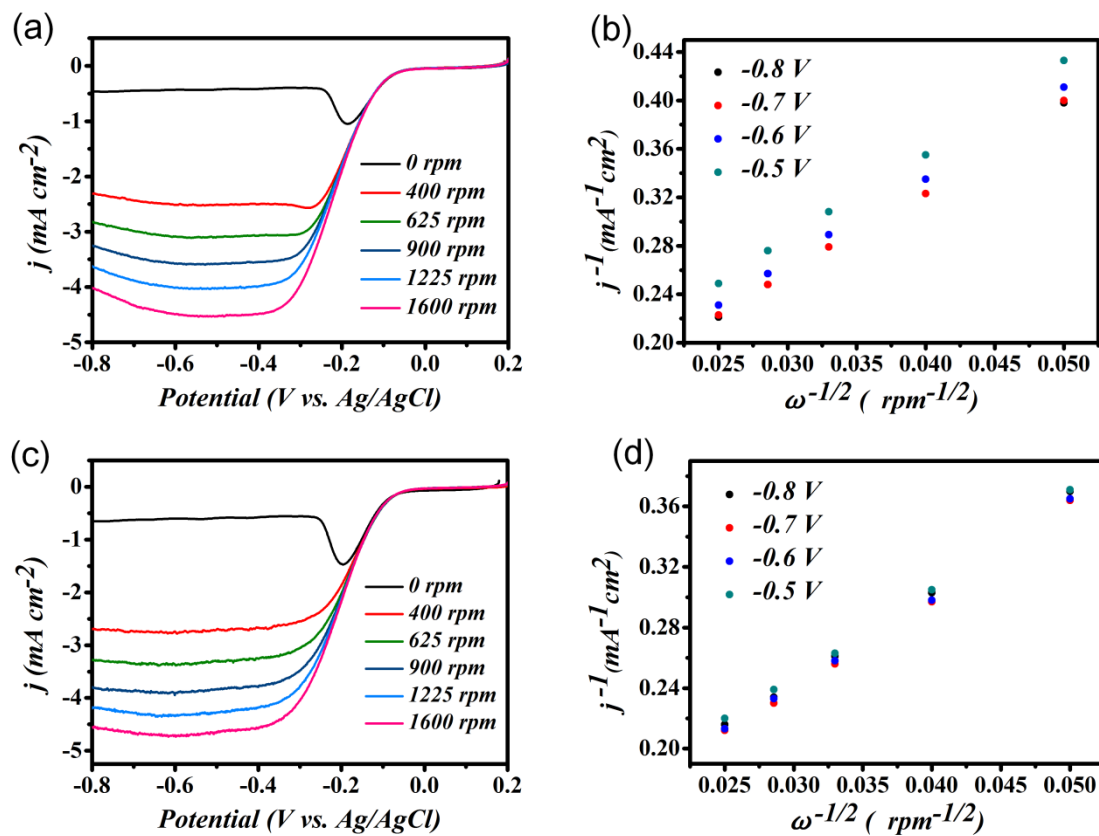


**Fig. S19** RDE curves of (a) N-GNs/CNT-A and (c) N-GNRs/CNT-A in an O<sub>2</sub>-saturated 0.1 M KOH solution with various rotation speeds at a scanning rate of 10 mV s<sup>-1</sup>. K-L plots of (b) N-GNs/CNT-A and (d) N-GNRs/CNT-A at different electrode potentials derived from RDE measurements.

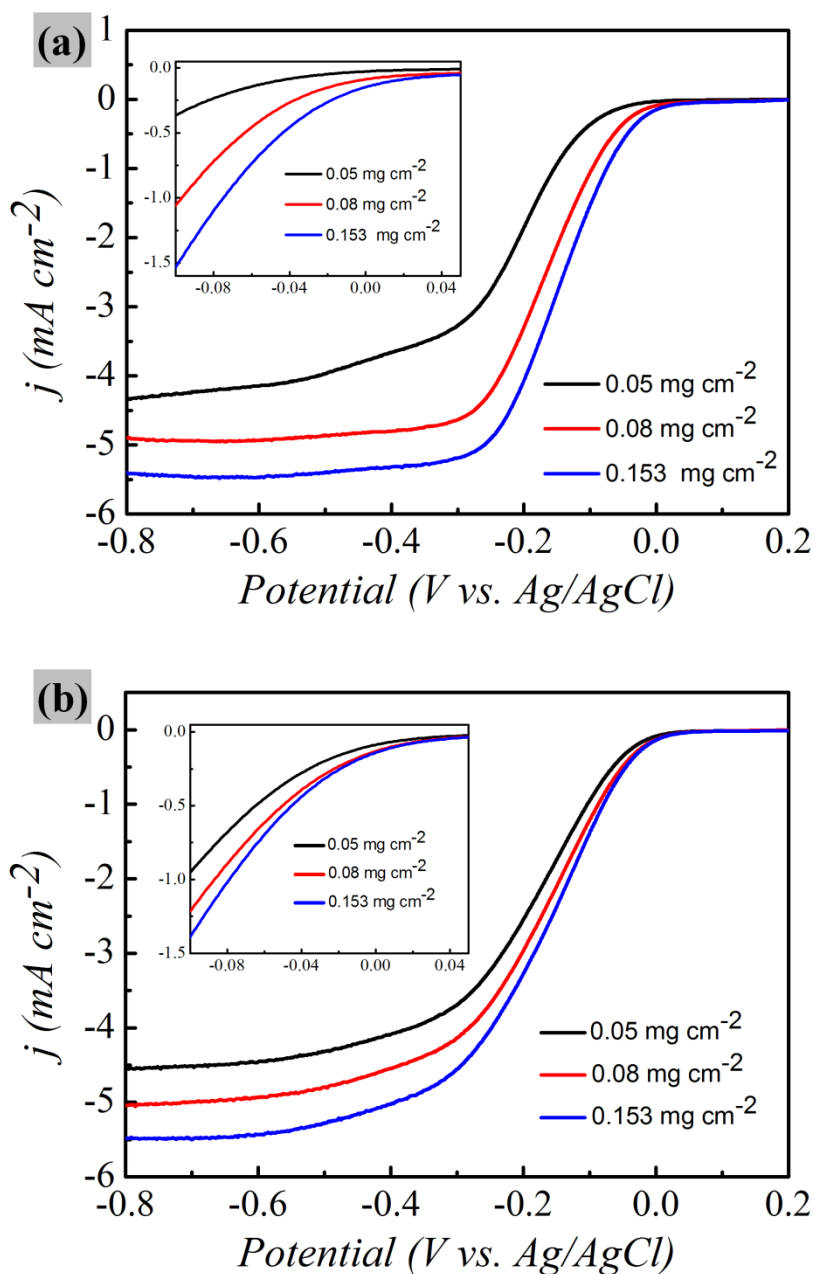


**Fig. S20** LSV curves of N-CNT@GNRs25-A (a) and N-CNT@GNRs85-A (b) with different mass loadings; the inset shows the onset potential of these samples.

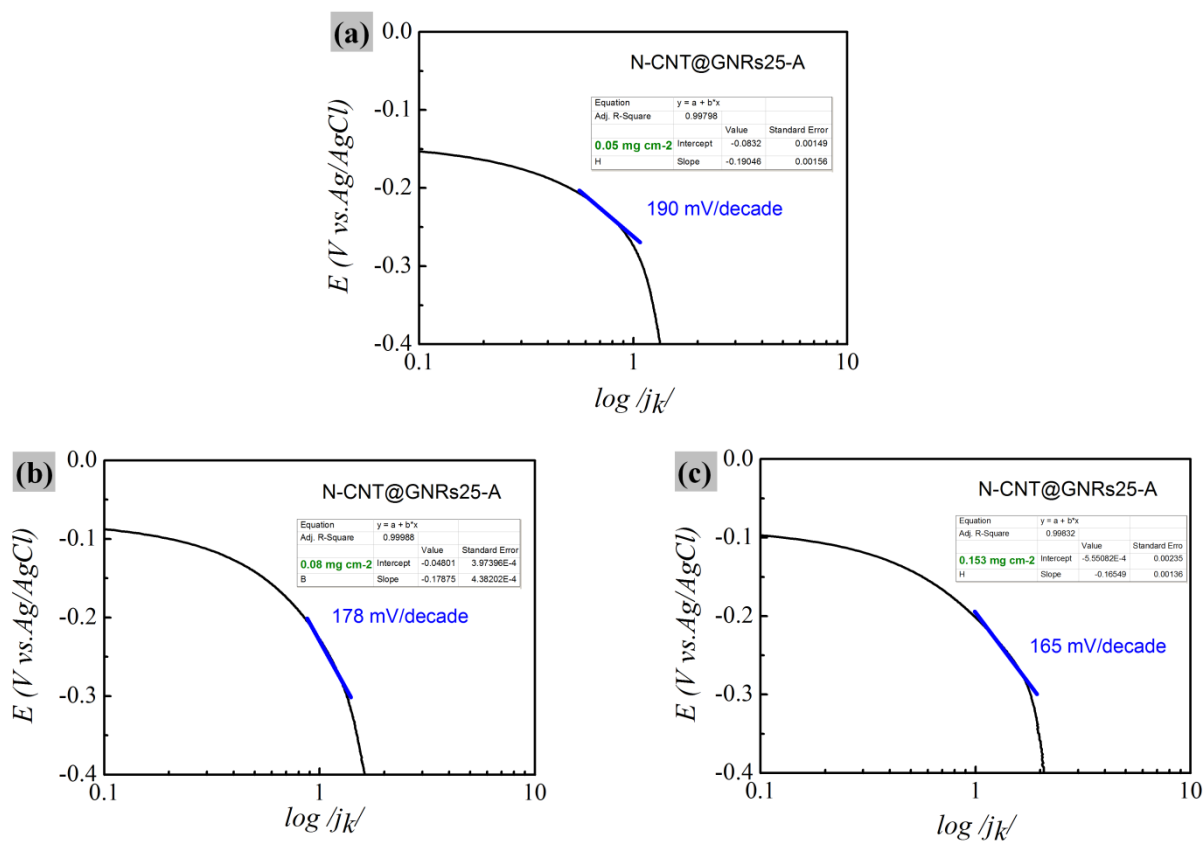


**Fig. S21** Tafel plots of the sample obtained from their LSV curves at 1600 rpm. **(a)** N-CNT@GNRs25-A with catalyst loading density of 0.05 mg cm<sup>-2</sup> on the 5 mm glass carbon electrode. **(b)** N-CNT@GNRs25-A with 0.08 mg cm<sup>-2</sup>. **(c)** N-CNT@GNRs25-A with 0.153 mg cm<sup>-2</sup>. Inset: The tables show the detailed parameters of fitting curves in the high overpotential regions.

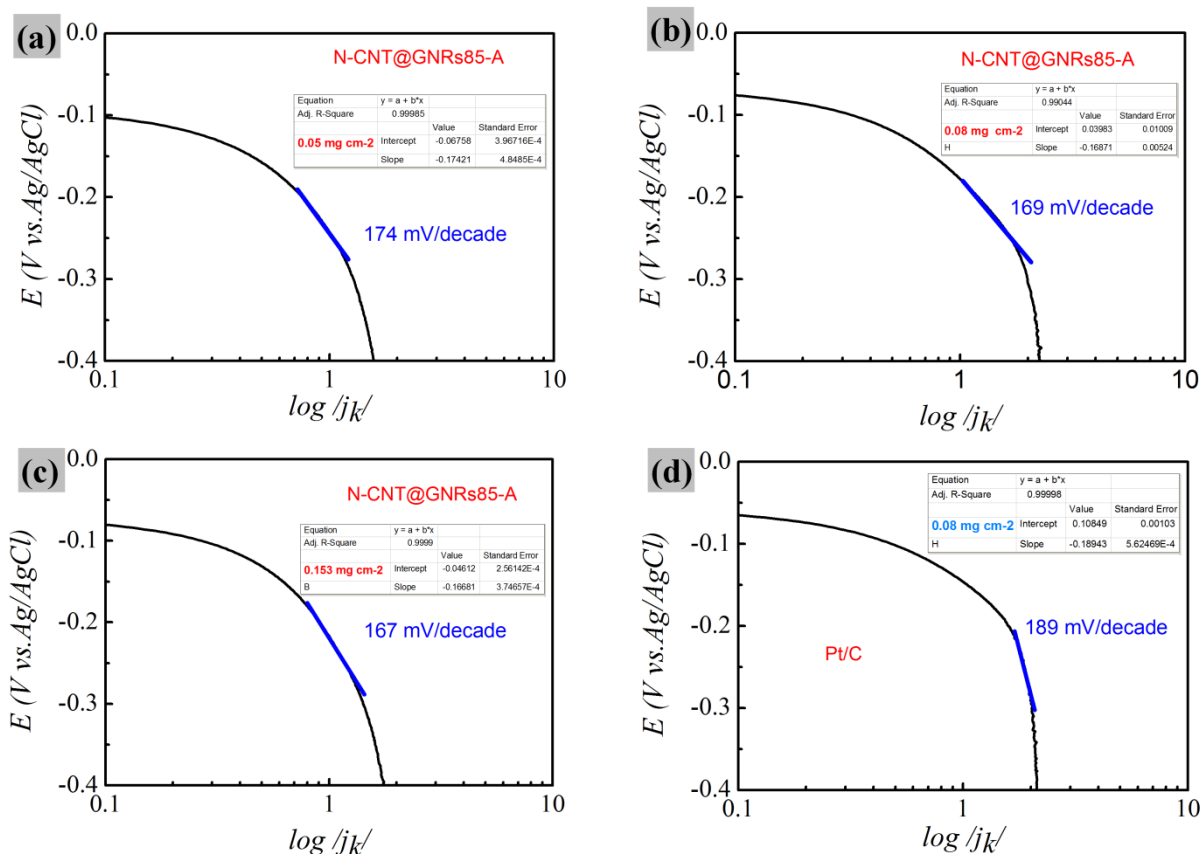


**Fig. S22** Tafel plots of the sample obtained from their LSV curves at 1600 rpm. **(a)** N-CNT@GNRs85-A with catalyst loading density of 0.05 mg cm<sup>-2</sup> on the 5 mm glass carbon electrode. **(b)** N-CNT@GNRs85-A with 0.08 mg cm<sup>-2</sup>. **(c)** N-CNT@GNRs85-A with 0.153 mg cm<sup>-2</sup>. **(d)** 20% Pt/C with 0.08 mg cm<sup>-2</sup> loading. Inset: The tables show the detailed parameters of fitting curves in the high overpotential regions.

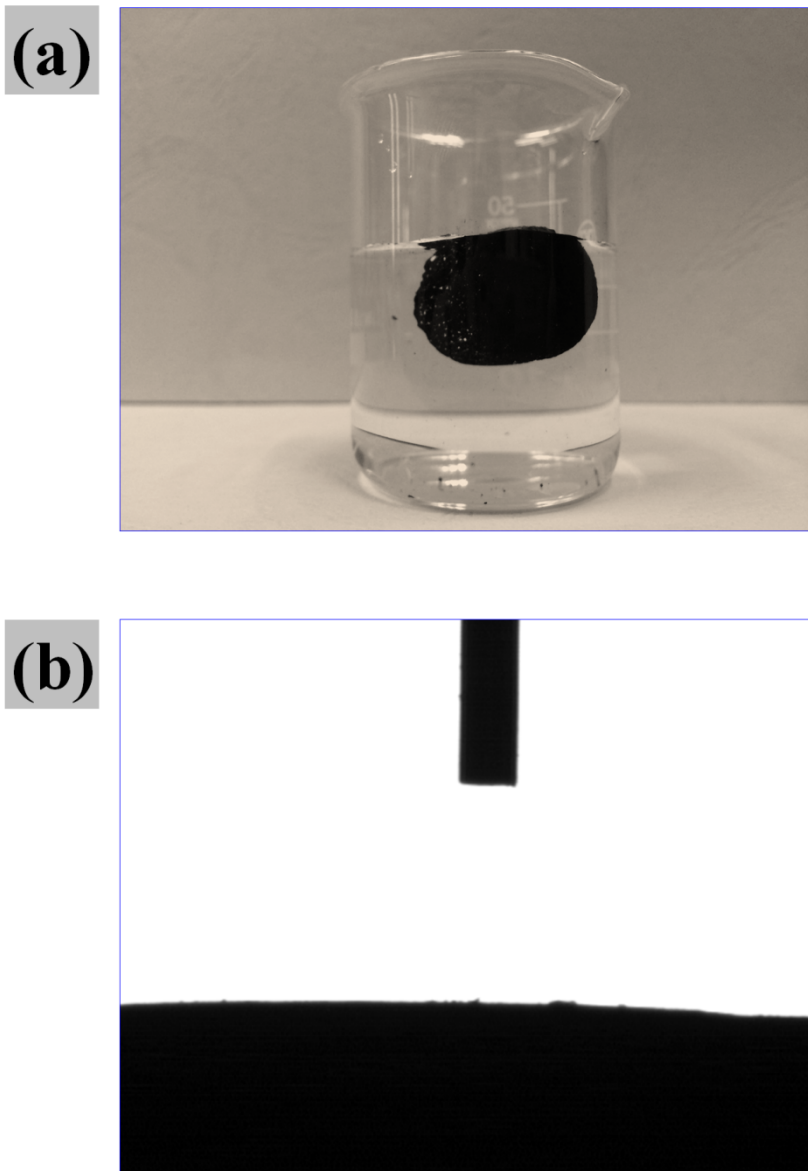


**Fig. S23 (a)** Digital photo showing the wetting behaviour of the N-CNT@GNRs85-A towards water. **(b)** The corresponding water contact angle of the aerogels surface.

As shown in Fig. S23, the prepared carbon nanoleaf aerogels were super-hydrophilic (its water contact angle is close to  $0^\circ$ ) due to incorporation of N atoms. While because of its ultralight nature, the aerogel for demonstration was float under the water instead of sinking to the bottom.

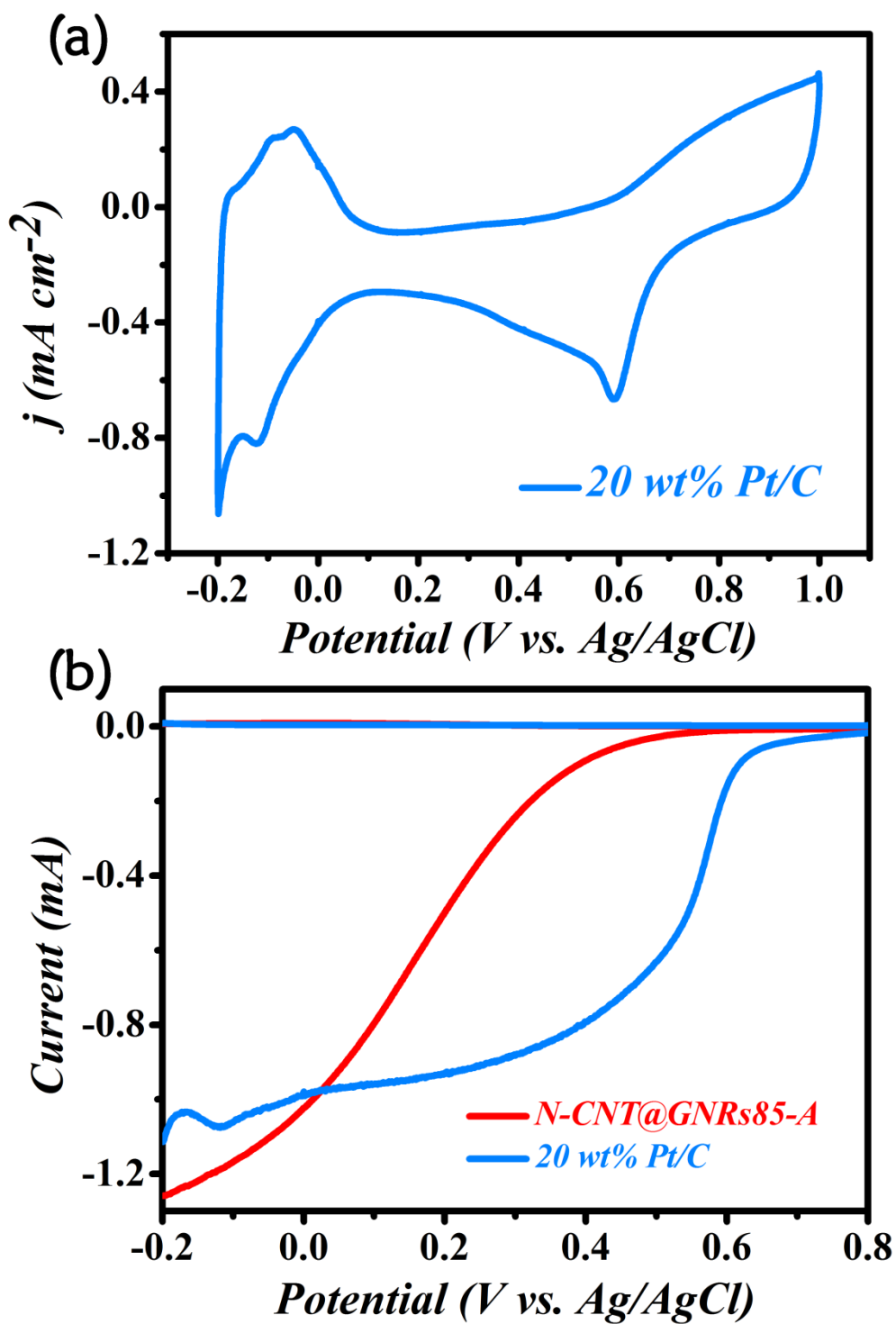


**Fig. S24** (a) CV curve of commercial Pt/C (20 wt%) in a  $\text{O}_2$ -saturated 0.5 M  $\text{H}_2\text{SO}_4$  solution at a scanning rate of  $10 \text{ mV s}^{-1}$ . (b) RRDE curves of N-CNT@GNRs85-A and Pt/C at 1600 rpm.

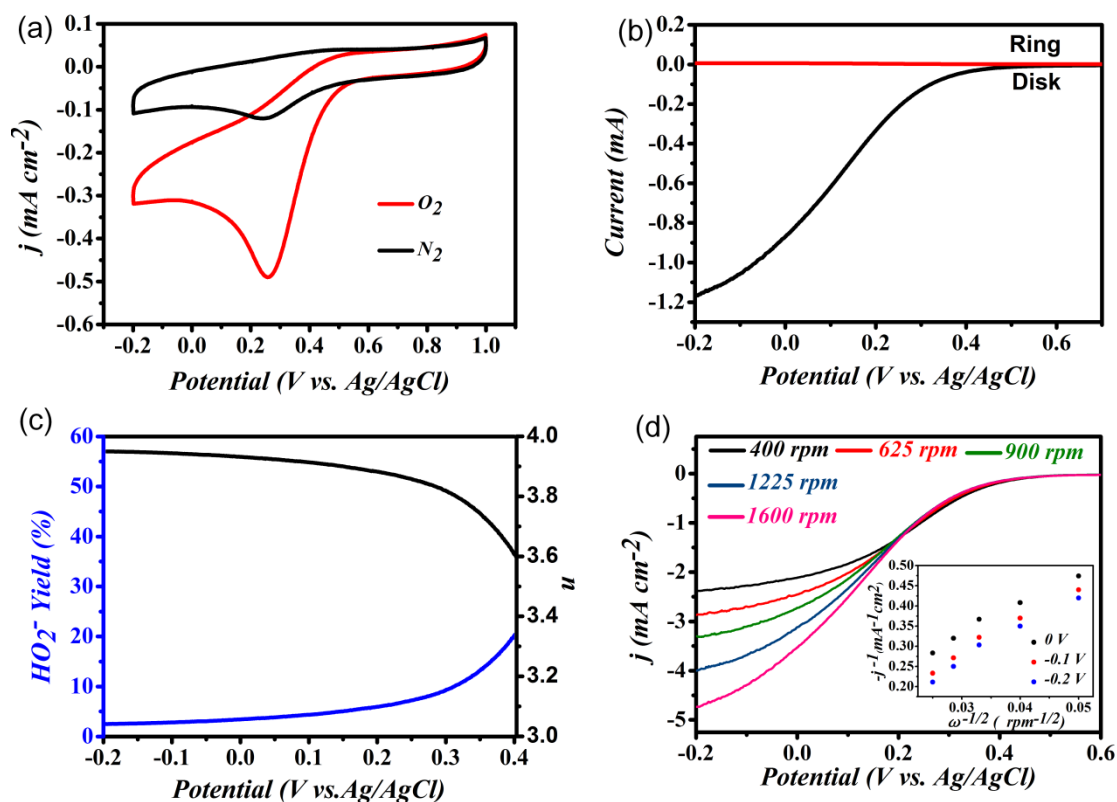


**Fig. S25** The ORR performance for N-GNRs/CNT-A in acidic solution. **(a)** CV curves of N-GNRs/CNT-A in an N<sub>2</sub>- and O<sub>2</sub>-saturated 0.5 M H<sub>2</sub>SO<sub>4</sub> solution, respectively, at scan rate of 10 mV s<sup>-1</sup>. **(b)** RRDE curves of the N-GNRs/CNT-A at 1600 rpm. **(c)** HO<sub>2</sub><sup>-</sup> production and the corresponding  $n$  values of the N-GNRs/CNT-A electrode. **(d)** LSV curves of N-GNRs/CNT-A in O<sub>2</sub>-saturated 0.5 M H<sub>2</sub>SO<sub>4</sub> solution at different rotating speeds. The scan rate is 10 mV s<sup>-1</sup>. Inset shows the  $K$ - $L$  plots derived from LSV curves at different potentials from -0.2 V~0V.

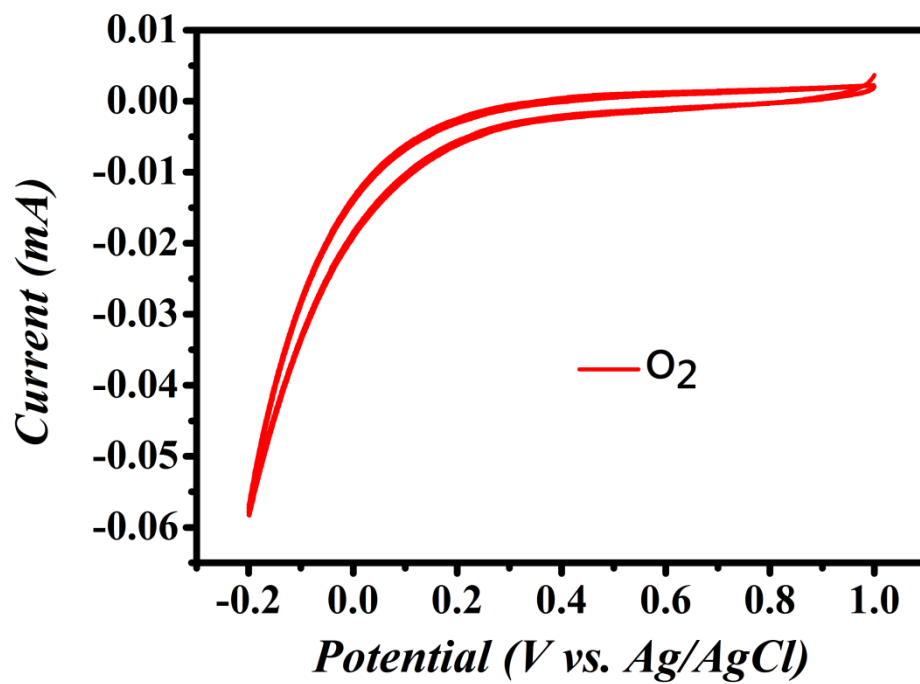


**Fig. S26** CV curves of N-GNs/CNT-A in an O<sub>2</sub>-saturated 0.5 M H<sub>2</sub>SO<sub>4</sub> solution, respectively, at scan rate of 10 mV s<sup>-1</sup>.

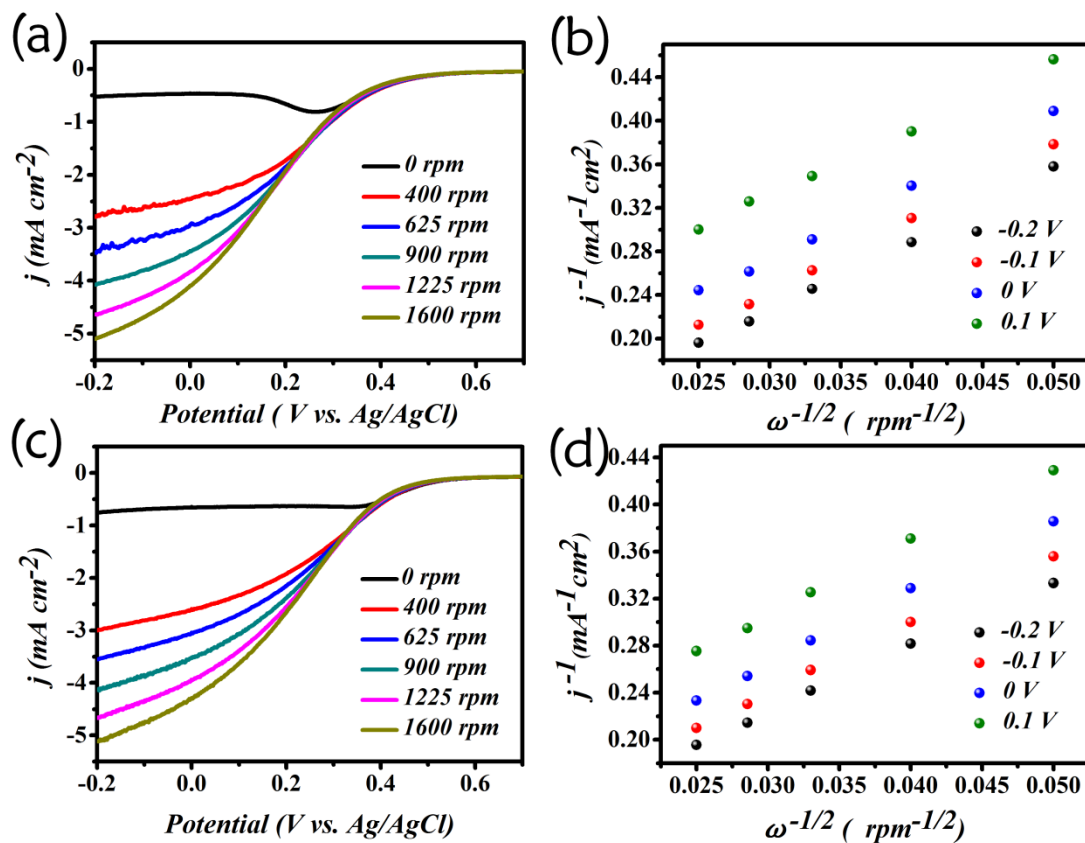


**Fig. S27** RDE curves of (a) N-CNT@GNRs25-A and (c) N-CNT@GNRs85-A in an O<sub>2</sub>-saturated 0.5 M H<sub>2</sub>SO<sub>4</sub> solution with various rotation speeds at a scanning rate of 10 mV s<sup>-1</sup>. K-L plots of  $J^{-1}$  vs.  $\omega^{-1/2}$  of (b) N-CNT@GNRs25-A and (d) N-CNT@GNRs85-A (with mass loading of 0.08 mg cm<sup>-2</sup>) at different electrode potentials derived from RDE measurements.

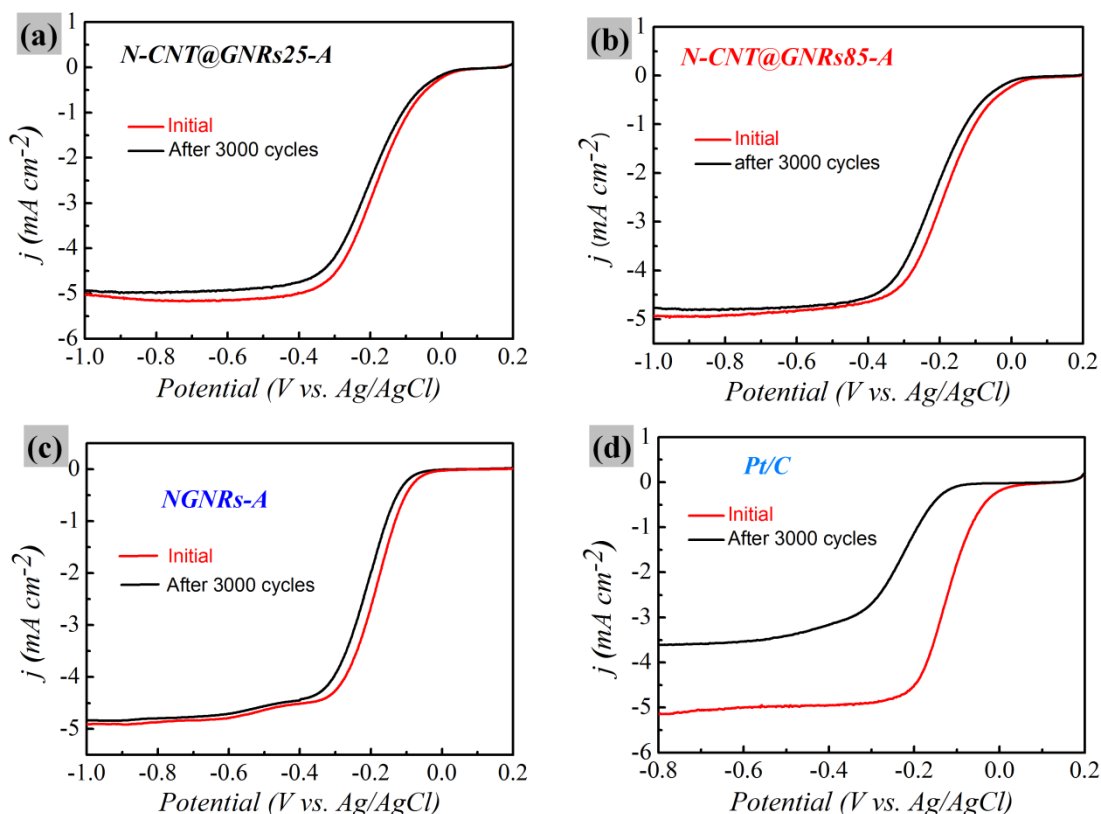


**Fig. S28** RRDE polarization curves of the (a) N-CNT@GNRs25-A, (b) N-CNT@GNRs85-A, (c) NGNRs-A and (d) Pt/C catalyst before and after 3000 potential cycles in O<sub>2</sub>-saturated 0.1 M KOH, respectively. Potential cycling was carried out between 0.2 V and -1.0 V versus Ag/AgCl at 100 mV s<sup>-1</sup>.

For the ADT test, 20 µg of the catalysts ink were loaded on to the RDE electrode with 5 mm glassy carbon disk. Before the start of the measurement, the electrolyte (0.1 M KOH) was bubbled with O<sub>2</sub> for 30 min. Then the CV test was conducted until the electrode reaches a steady state. After that, the RDE measurement was conducted at a rotating speed of 1600 rpm at a scan rate of 10 mV s<sup>-1</sup>. Then the electrode was performed an accelerated CV test in O<sub>2</sub>-saturated 0.1 M KOH for 3000 cycles at a scan rate of 100 mV s<sup>-1</sup>, the RDE measurement was conducted again at a rotating speed of 1600 rpm at a scan rate of 10 mV s<sup>-1</sup>. Obviously, negligible negative shift in the half-wave potential were observed for two kinds of carbon nanoleaf aerogels (N-CNT@GNRs25-A and N-CNT@GNRs85-A) and N-GNRs-A, while the Pt/C catalyst displayed an inferior durability with obviously cathodic current loss accompany with negative shift in both the half-wave potential and onset potential after 3000 potential cycles between 0.2V and -1.0V.

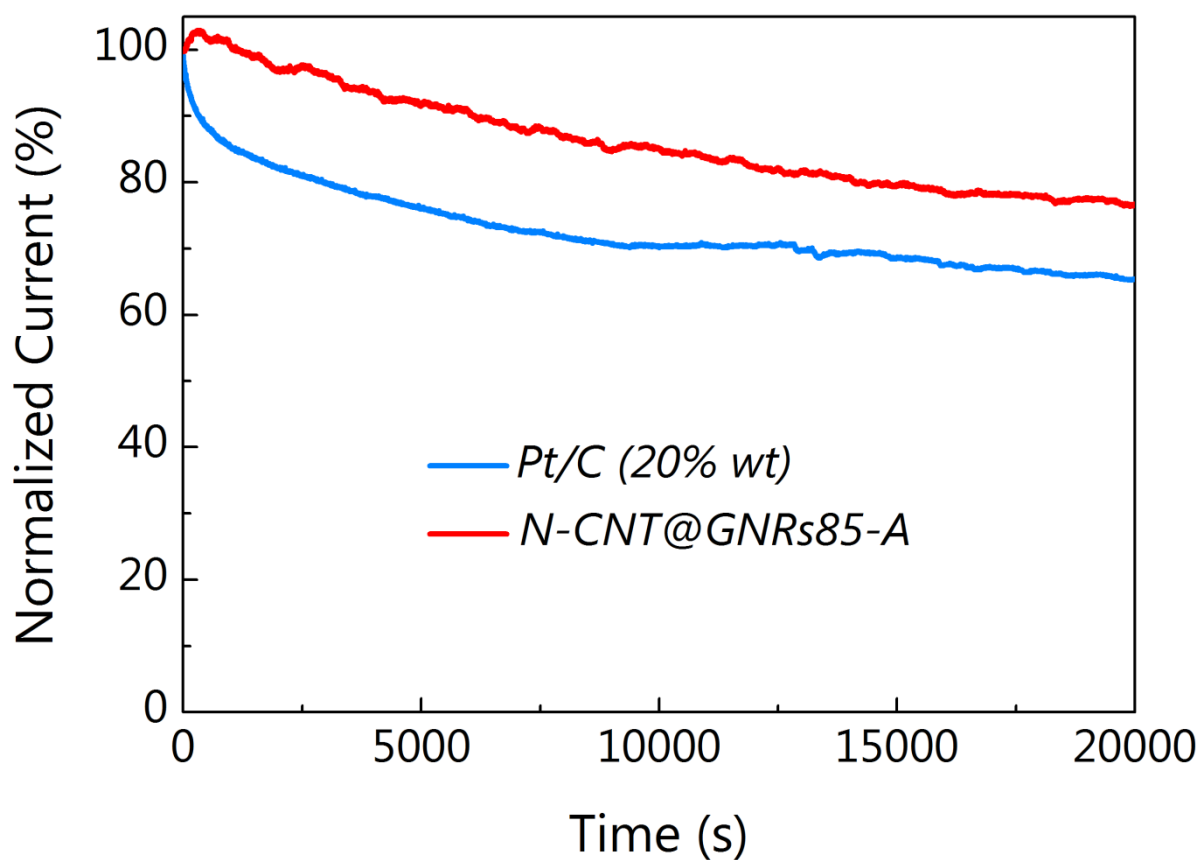


**Fig. S29** Current-time (i-t) chronoamperometric response of the N-CNT@GNRs85-A and Pt/C electrodes at 0.40 V (vs Ag/AgCl) in O<sub>2</sub>-saturated 0.5 M H<sub>2</sub>SO<sub>4</sub> solution at a rotation rate of 1600 rpm.

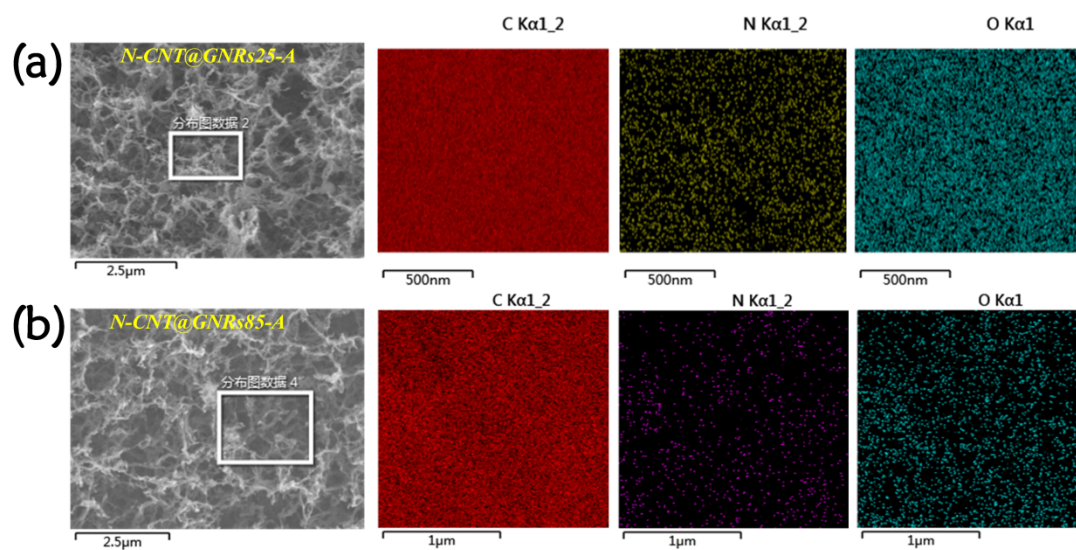


**Fig. S30** EDS image and elemental mapping of (a) N-CNT@GNRs25-A and (b) N-CNT@GNRs85-A.

## Reference:

- [s1] P. Chen, T. Y. Xiao, Y. H. Qian, S. S. Li, and S. H. Yu, *Adv. Mater.*, 2013, **25**, 3192-3196.
- [s2] Z. Sui, Q. Meng, X. Zhang, R. Ma, and B. Cao, *J. Mater. Chem.*, 2012, **22**, 8767-8771.
- [s3] L. Chen, R. Du, J. H. Zhu, Y. Y. Mao, C. Xue, N. Zhang, Y. L. Hou, J. Zhang, and T. Yi, *Small*, 2014, **10**, DOI: 10.1002/ smll. 201402472R1.
- [s4] K. Parvez, S. B. Yang, Y. Hernandez, A. Winter, A. Turchanin, X. L. Feng, and K. Müllen, *ACS Nano*, 2012, **11**, 9541-9550.
- [s5] Z. H. Sheng, L. Shao, J. J. Chen, W. J. Bao, F. B. Wang, and X. H. Xia, *ACS Nano*, 2011, **5**, 4350-4358.
- [s6] C. Zhang, R. Hao, H. Liao, and Y. Hou, *Nano Energy* 2013, **2**, 88-97.
- [s7] I. Y. Jeon, D. S. Yu, S. Y. Bae, H. J. Choi, D. W. Chang, L. M. Dai, and J. B. Baek, *Chem. Mater.*, 2011, **23**, 3987-3992.
- [s8] Z. Lin, M. K. Song, Y. Ding, Y. Liu, M. Liu, and C. Wong, *Phys. Chem. Chem. Phys.*, 2012, **14**, 3381-3387.
- [s9] Y. Li, Y. Zhao, H. H. Cheng, Y. Hu, G. Q. Shi, L. M. Dai, and L. T. Qu, *J. Am. Chem. Soc.*, 2012, **134**, 15-18.
- [s10] Z. Lin, G. Waller, Y. Liu, M. Liu, and C.P. Wong, *Adv. Energy Mater.*, 2012, **2**, 884-888.
- [s11] Y. Zhao, C. G. Hu, Y. Hu, H. H. Cheng, G. Q. Shi, and L. T. Qu, *Angew. Chem. Int. Ed.*, 2012, **124**, 11533-11537.
- [s12] S. B. Yang, L. J. Zhi, K. Tang, X. L. Feng, J. Maier, and K. Müllen, *Adv. Funct. Mater.*, 2012, **22**, 3634-3640.
- [s13] P. Chen, T. Y. Xiao, Y. H. Qian, S. S. Li, and S. H. Yu, *Adv. Mater.*, 2013, **25**, 3192-3196.
- [s14] Z. H. When, S. Ci, Y. Hou, and J. Chen, *Angew. Chem. Int. Ed.*, 2014, **53**, 6496-6500.
- [s15] J. Liang, Y. Jiao, M. Jaroniec, and S. Z. Qiao, *Angew. Chem. Int. Ed.*, 2012, **51**, 11496-11500.
- [s16] I. Y. Jeon, S. Zhang, L. Zhang, H. J. Choi, J. M. Seo, Z. H. Xia, L. M. Dai, and J. B. Baek, *Adv. Mater.*, 2013, **25**, 6138-6145.
- [s17] M. Liu, Y. Song, S. He, W. W. Tjiu, J. Pan, Y. Y. Xia, and T. X. Liu, *ACS Appl. Mater. Interfaces*, 2014, **6**, 4214-4222.

- [s18] S. Chen, J. Bi, Y. Zhao, L. Yang, C. Zhang, Y. Ma, Q. Wu, X. Wang, and Z. Hu, *Adv. Mater.*, 2012, **24**, 5593-5597.
- [s19] J. Xu, Y. Zhao, C. Shen, and L. Guan, *ACS Appl. Mater. Interfaces*, 2013, **5**, 12594-12601.
- [s20] J. Xu, G. Dong, C. Jin, M. Huang, and L. Guan, *ChemSusChem*, 2013, **6**, 493-499.
- [s21] Y. Zhao, C. G. Hu, L. Song, L. Wang, G. Q. Shi, L. M. Dai, and L. T. Qu, *Energy Environ. Sci.*, 2014, **7**, 1913-1918.
- [s22] Y. Xue, D. Yu, L. Dai, R. Wang, D. Li, A. Roy, F. Lu, H. Chen, Y. Liu, and J. Qu, *Phys. Chem. Chem. Phys.*, 2013, **15**, 12220-12226.
- [s23] S. Wang, E. Iyyamperumal, A. Roy, Y. Xue, D. S. Yu, and L. M. Dai, *Angew. Chem. Int. Ed.*, 2011, **50**, 11756-11760.
- [s24] K. Gong, F. Du, Z. H. Xia, M. Durstock, and L. M. Dai, *Science*, 2009, **323**, 760-764.
- [s25] W. Wei, H. W. Liang, K. Parvez, X. Zhuang, X. L. Feng, and K. Müllen, *Angew. Chem. Int. Ed.*, 2014, **53**, 1570-1574.
- [s26] Y. Wang, X. Jiang, *ACS Appl. Mater. Interfaces*, 2013, **5**, 11597-11602.
- [s27] W. Yang, T. P. Fellingner, and M. Antonietti, *J. Am. Chem. Soc.*, 2011, **133**, 206-209.
- [s28] C. Hu, Y. Xiao, Y. Zhao, N. Chen, Z. Zhang, M. Cao, and L. T. Qu, *Nanoscale*, 2013, **5**, 2726-2733.
- [s29] J. Liang, X. Du, C. Gibson, X. W. Du, and S. Z. Qiao, *Adv. Mater.*, 2013, **25**, 6226-6231.